Physical metallurgy of a Ti–5%Ta–1.8%Nb alloy

Article *in* Transactions of the Indian Institute of Metals · October 2012

DOI: 10.1007/s12666-008-0070-x

3 authors:

Saroja Saibaba
Indira Gandhi Centre for Atomic Research
216 PUBLICATIONS **2,644** CITATIONS
SEE PROFILE

M. Vijayalakshmi
Srimad Andavan Arts & Science College
165 PUBLICATIONS **2,164** CITATIONS
SEE PROFILE

Baldev Raj
Indira Gandhi Centre for Atomic Research
919 PUBLICATIONS **18,386** CITATIONS
SEE PROFILE

Trans Indian Inst Met (April 2012) 65(2):111–133
DOI 10.1007/s12666-011-0114-5

OVERVIEW PAPER

Ti–5Ta–1.8Nb: An Advanced Structural Material for High Performance Application in Aggressive Oxidising Environments

S. Saroja · M. Vijayalakshmi · Baldev Raj

Received: 3 May 2011 / Accepted: 26 December 2011 / Published online: 12 April 2012

Abstract It is well known that Ti and Zr based alloys are best suitable for oxidizing environments due to their superior corrosion resistance. This has been exploited in the development of the ternary Ti–Ta–Nb alloy, for the dissolver in a fast reactor fuel reprocessing plant, the efforts of which are summarized in the present overview. Closing of fuel cycle is a priority for the three stage nuclear power program of India, towards which, indigenous development of reprocessing technology and materials is an important milestone. Corrosion resistance of structural materials controls the operating life of the dissolver in a nuclear reprocessing plant, where the spent nuclear fuel is dissolved in highly oxidizing boiling nitric acid. A complete physical metallurgy database of the alloy has been generated to understand the various phase transformations and the resultant microstructures. Corrosion control in different phases of nitric acid is achieved through microstructural optimization and the mechanisms of corrosion are understood using a detailed study of passive oxide film. The dependence of transformation texture on the mode of deformation and the role of severe plastic deformation on mechanical properties have been elucidated. These extensive R&D efforts resulted in a complete understanding of the metallurgy the alloy, which is discussed in this overview.

Keywords Fast reactor fuel reprocessing · Titanium · Phase transformations · Microstructure · Corrosion resistance · Texture · Severe plastic deformation

S. Saroja · M. Vijayalakshmi (✉)
Indira Gandhi Centre for Atomic Research,
Kalpakkam 603102, Tamilnadu, India
e-mail: mvl@igcar.gov.in

B. Raj
PSG Institutions, Coimbatore, Tamilnadu, India

1 Introduction

Corrosion has been one of the common problems, ever since the interaction between man and metal started in the human civilization. The materials were selected by trial and error, much before the metallurgical sciences and technology matured into a well documented universally accessible and acceptable form of information and knowledge. Despite these limitations, there are many archeological marvels, like the famous iron pillar at Delhi [1], which have stood the test of time under different climatic and environmental conditions.

The genesis of deliberate design of corrosion resistant alloys can be traced to the discovery of 'galvanic series' and the concept of Pourbaix diagram. The Nernst equation used to determine the potential that develops during the oxidation–reduction reaction at the anode and cathode of the electrochemical cell is used to construct the Pourbaix diagram. Titanium, occupies an advantageous position in the Pourbaix diagram, suggesting its suitability for the process industries. Hence, extensive research and development efforts have been diverted in the last century to extract the best potential of titanium and its alloys. As a result, a large number of commercial alloys, suitable for many industries, have been developed (Fig. 1).

Ti forms a passive oxide layer which is protective and is responsible for its superior corrosion-resistance. The stable oxide is titanium dioxide, TiO_2, and the lower oxides of Ti_2O_3 and TiO are also seen under weakly oxidizing conditions [2]. The usable range of different alloys in acidic medium is given in Fig. 2 [3], which shows that corrosion resistance of Ti is rather poor in reducing acids. The extensive research efforts have been summarized in a large number of review articles in recent years in many books and international journals [4–8].

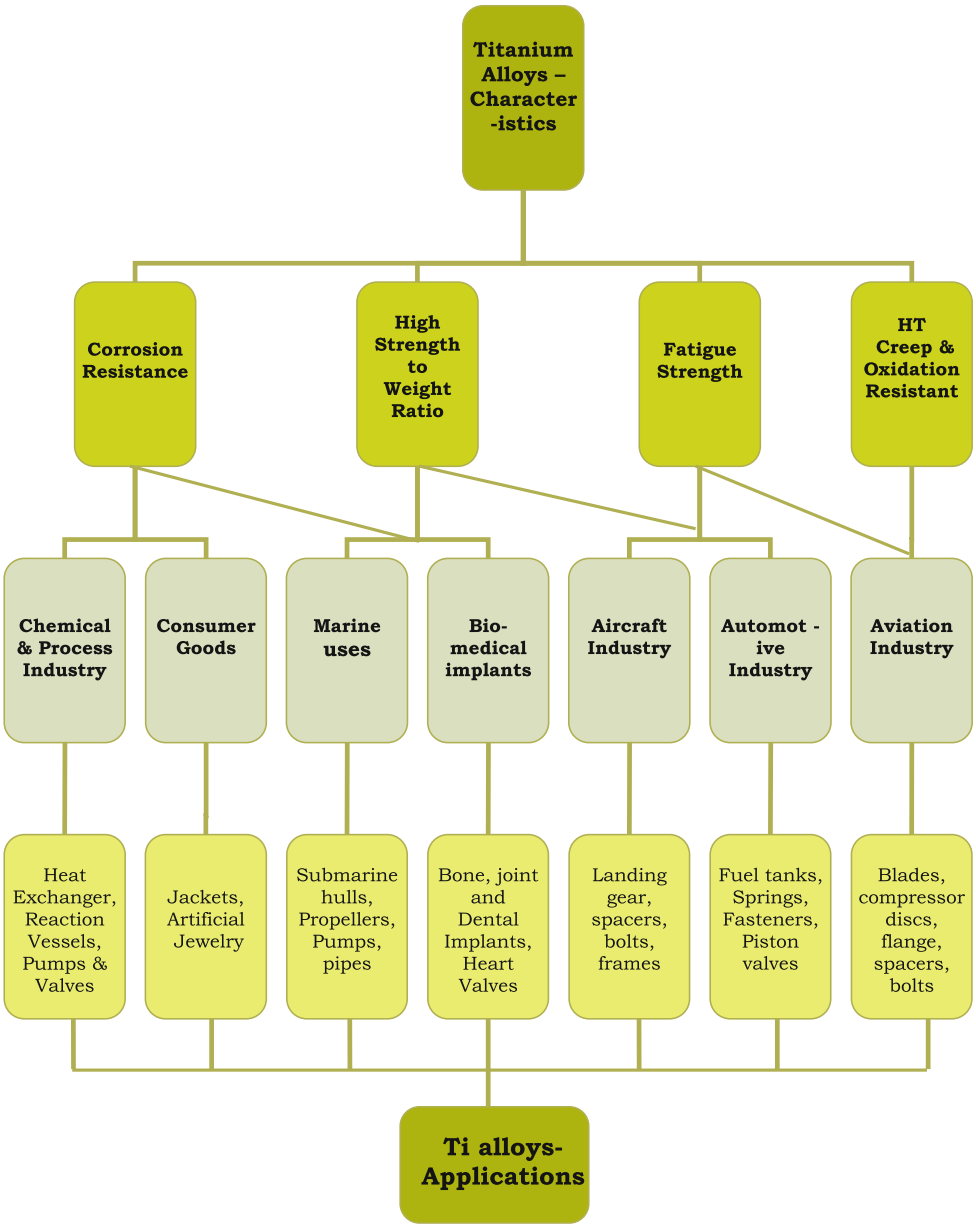

Fig. 1 General characteristics and typical applications of titanium alloys. (Color figure online)

The excellent corrosion resistance of Ti and its alloys has been best utilized in several industries ranging from military, aerospace, automobile, petro-chemical and marine applications. Nuclear industry is yet another domain where the potentials of Ti alloy can best be exploited, especially in the back end of the fuel cycle. Closing the fuel cycle has been a major priority in the three stage Indian Nuclear Power Program, which is an important step in bringing down the overall cost of power production, with the additional advantages of alternate fuel resources and better waste management. One of the thrust areas of research at Indira Gandhi Centre for Atomic Research, Kalpakkam has been the indigenous development of technology and materials for the fast reactor fuel cycle.

It is necessary to develop advanced materials better than commercial grades of Ti or nitric acid grade SS for dissolution of spent nuclear fuel in reprocessing applications [9]. Earlier studies of corrosion behavior of candidate materials in boiling nitric acid have identified four different classes of alloys suitable for use in boiling nitric acid medium. These include low carbon 300 series stainless steel, high Cr, Ni-based alloys, Ti and Zr based alloys [9–13]. A comparison of corrosion rates of these alloys is given in Fig. 3 [14]. It is observed that titanium and zirconium alloys show low corrosion rates in hot, concentrated nitric acid. The performance of titanium and zirconium alloys in nitric acid medium has been extensively studied and is compared in Table 1 [10, 14–21].

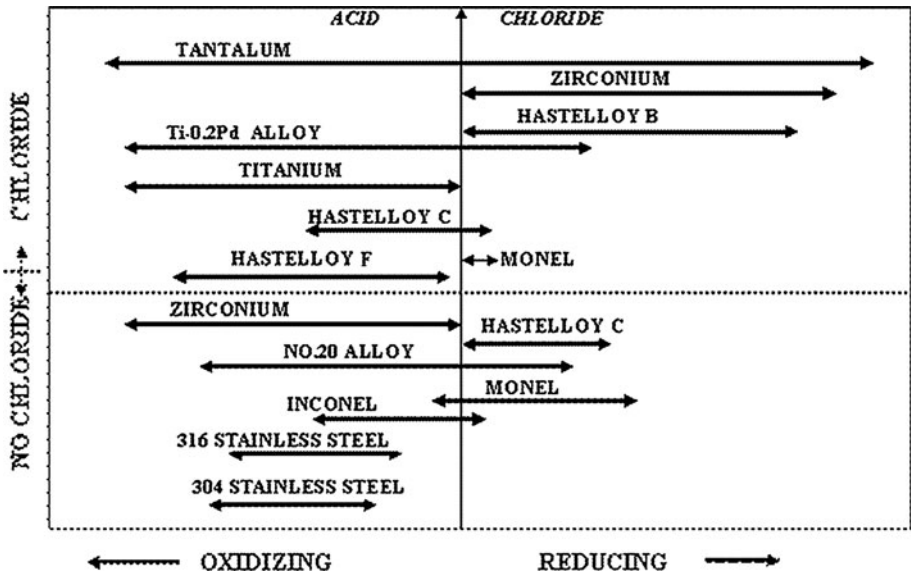

Fig. 2 Comparison of corrosion properties of different alloys in oxidizing and reducing media [3]

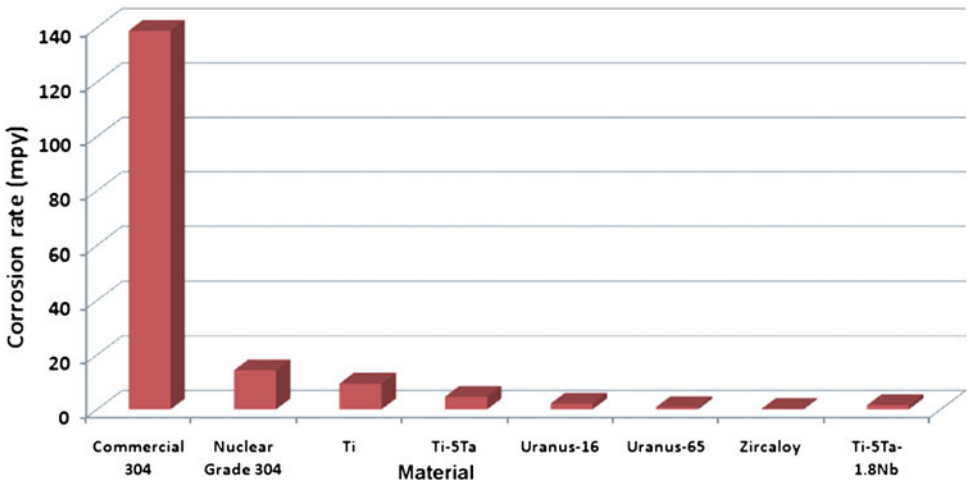

Fig. 3 Comparison of corrosion rate of stainless steels, Ti alloys and zircaloy in nitric acid of 11.5 M concentration. (Color figure online)

Table 1 Comparison of titanium and zirconium alloys in nitric acid

S. No	Property	Zr/Zr alloys	Ti/Ti alloys
1.	Corrosion resistance in 65–70% boiling HNO_3	Good	Good
2.	Change in corrosion resistance with concentration of HNO_3	Nearly constant up to 70%	Shows maximum corrosion rate in the mid range (40–50%) of concentrations
3.	Effect of purity of HNO_3	Does not influence	With increase in purity, corrosion resistance decreases, since trace amount of impurities act as inhibitors
4.	Stress corrosion cracking (SCC)	Prone for SCC especially HAZ of weldments	No SCC
5.	Condensate phase corrosion	No	Major problem
6.	Change of passive to transpassive corrosion	At concentrations >40%, these regions come closer and this may lead to SCC	No such transition
7.	Texture	Corrosion fatigue accelerated w.r.t texture	Texture has less effect on corrosion fatigue due to higher number of slip systems available
8	Presence of Fe	–	Corrosion rate increases beyond 0.05 wt%
9.	Corrosion fatigue in HNO_3	Only {1010} slip system and hence prone for corrosion fatigue	Multiple slip systems and less probability

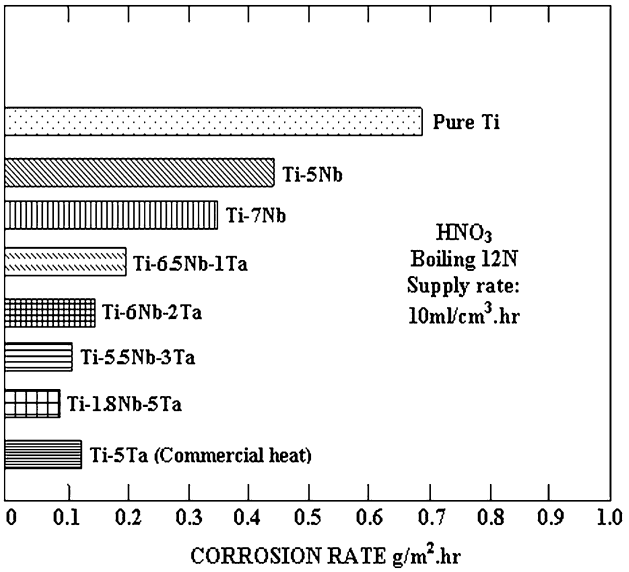

Fig. 4 Comparison of corrosion rate of Ti and its alloys in nitric acid [10]

For oxidizing environments titanium with various compositions of Ta and Nb has been evaluated by Kiuchi et al. [10]. The comparison of different alloys is shown in Fig. 4 [10]. It can be seen that Ti–5%Ta–1.8%Nb alloy displays the best corrosion resistance in boiling 12 N nitric acid. In fact, the corrosion resistance of pure Ti, Ti–5Ta and Ti–5%Ta–1.8%Nb alloy increases in the ratio 1:1.5:7. Hence, in view of the high corrosion resistance of Ti–5%Ta–1.8%Nb alloy, it is considered to be a potential candidate material for structural applications such as vessels for dissolvers and evaporators in nuclear fuel reprocessing plants [10, 14] and has been taken up for a detailed study. An indigenous effort to develop the ternary Ti–Ta–Nb alloy as a candidate structural material for the dissolver in a fast reactor fuel reprocessing plant has been undertaken. These studies are discussed in the present overview.

2 Development of Ti–5%Ta–1.8%Nb Alloy

A detailed study has been carried out with respect to processing, fabrication, weldability and evaluation of properties for the alloy. The Ti–Ta–Nb alloy of composition (4.39 wt% Ta, 1.85 wt% Nb and Ti, with Fe, O, N, C and H of 263, 500, 47, 125 and 9 ppm respectively) has been produced in collaboration with MIDHANI and Nuclear Fuel Complex, Hyderabad, in various product forms such as plates, rods and wires.

It is known that Ti alloys possess a variety of microstructures which can be tailored by appropriate phase transformations of the high temperature b.c.c. β phase. The mode of phase transformations in Ti alloys is strongly influenced by alloy chemistry, and process conditions such as temperature and cooling rate [22, 23]. The versatility of Ti alloys stems from this ability to achieve the desired properties through microstructure control vis-a vis design of appropriate thermo-mechanical or thermal treatments. The Ti–5Ta–1.8Nb being a new alloy had very scarce information even on fundamental characteristics like transformation behavior and temperatures. An indepth study has been carried out to understand the behaviour of this alloy, w.r.t. transformation characteristics, the microstructure evolution and consequent impact on the properties.

2.1 Physical Metallurgy of Ti–5Ta–1.8Nb Alloy

Pure Titanium exhibits allotropic transformation from bcc-β to hcp-α when cooled below 1155 K. Most of the Ti alloys are classified into either α or $\alpha + \beta$ or β alloys, based on the stable room temperature microstructure. Addition of β stabilizing alloying elements (such as Ta, Nb) decreases the transformation temperature and also widens the two phase field regime. The alloy of interest in the present study, Ti–5Ta–1.8Nb has been classified as a $\alpha + \beta$ alloy [24] based on the retention of $\sim$13% of β phase at room temperature, when the high temperature β phase undergoes a Widmanstatten transformation [25] to result in a lamellar $\alpha + \beta$ microstructure (Fig. 5). The β coexisting with α is enriched with Ta and Nb, due to availability of sufficient time for repartitioning during slow cooling. The β transus and martensite start temperature has been determined for the first time for this alloy using a variety of techniques like electron microscopy, differential scanning calorimetry and empirical equations. Based on metallography analysis of the products cooled from a range of temperatures above 1000 K the β transus for this alloy was estimated to lie between 1138 and 1143 K [24]. A Differential Scanning Calorimetry experiment carried out to determine the onset of β transformation and the β transus for this alloy showed the onset of β at about 1092 K and β transus is at about 1138 K [24]. Additionally, T_β was calculated by an empirical method, based on β stabilizing efficiencies of different alloying elements [26], which suppressed the $\alpha \rightarrow \beta$ transformation temperature relative to that of pure Ti. This suppression was 7.22, 2.22 and 17.78 K [26] for every weight percent of niobium, tantalum and iron respectively. The β transus evaluated by this method was about 1133 K [24], which agrees well with that evaluated experimentally.

The M_s temperature of pure titanium is 1128 K and is reported to be very sensitive to the amount of β stabilizers [27, 28]. Suppression of M_s temperature of pure titanium for each w% addition of Ta, Nb, Mo and Fe was estimated as 4.5, 10.5, 26.25 and 90.5 K respectively, based on

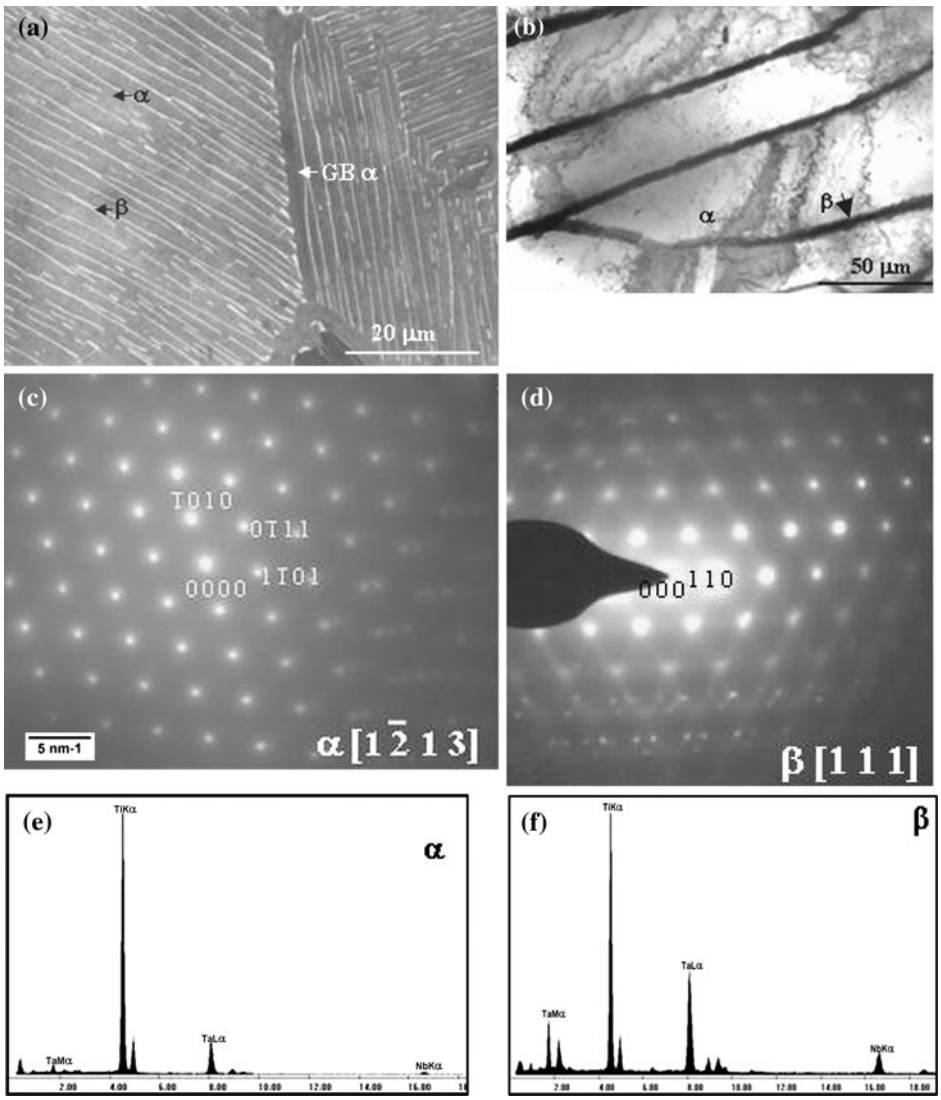

Fig. 5 Microstructure of as cast alloy showing **a** GBα and uniformly acicular 'transformed β structure'; **b** well resolved individual lamellae of α and β phases; **c**, **d** SAD patterns of hcp α (**c**) and bcc β phases (**d**) along zone axis $[1\bar{2}13]$ and [111] respectively; and **e**, **f** EDS spectra showing enrichment of Ta and Nb in β as compared to α phase

which, M_s temperature was calculated to be 1086.5 K [24], from the Nb and Ta content as well as using the Mo equivalent of the alloy. These two temperatures enabled the selection of hot working temperature of the alloy and a safe operating window of 1103–1113 K was recommended for the process.

2.2 Phase Transformations in Ti–5Ta–1.8Nb Alloy

The distinct transformation mechanisms that take place during cooling of β phase through α + β phase filed (973–1143 K) established the role of solute content and cooling rate in determining the stability of high temperature β phase. A wide spectrum of microstructures, which possessed characteristic features with respect to morphology, crystal structure and microchemistry could be arrived at, which is described in detail below.

2.2.1 *Microstructural Modification During Thermomechanical Processing*

The high temperature β phase of Ti–Ta–Nb alloy resulted always in a lamellar α + β structure on slow cooling. The only means of arriving at an equiaxed microstructure is by 'breaking' the lamellar product through 'deformation' of α + β lamellar product, followed by annealing in the α + β phase field. The Ti–Ta–Nb alloy with lamellar α + β structure, when subjected to a hot deformation in two phase field (dynamic recrystallisation) or subsequent cold deformation of the β processed alloy, followed by two phase anneal, resulted in a microstructure consisting of predominantly polygonal α with small amount of isolated β particles. This microstructure shown in Fig. 6a, b is obtained by the culmination of a series of processing stages which is depicted in the schematic in Fig. 6c. Hot extrusion

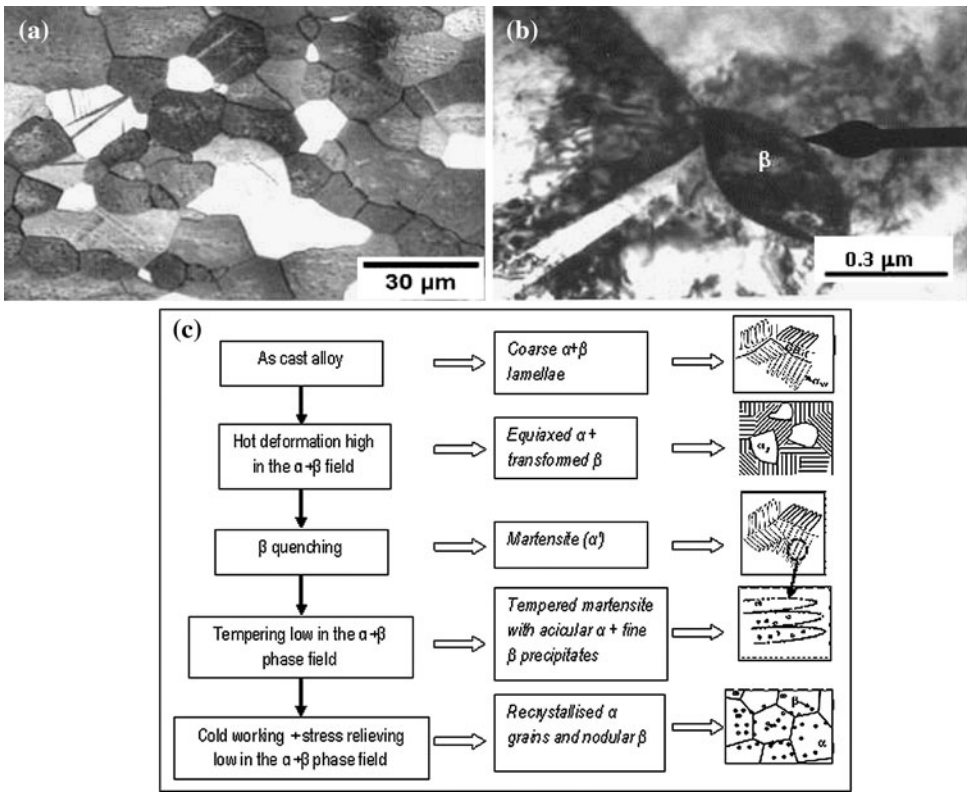

Fig. 6 Microstructure of the thermo-mechanically processed alloy showing **a** an equiaxed structure; **b** equiaxed primary α and β precipitate at the α grain boundary; and **c** schematic of flow chart followed for obtaining a microstructure with recrystallised α grains and nodular β in a Ti–5%Ta–1.8%Nb alloy

(stage 1) of the lamellar structure in the two phase field, is known to result in a bimodal structure of equiaxed primary α in a transformed β matrix [29]. The isolated fine β particles observed along lath boundaries and substructures in the α matrix suggests that the β phase forms as a consequence of the tempering of martensite after β quenching (stage 2). It is reported [23] that though h.c.p. α' forms in both isomorphous and eutectoid systems on β quenching, the products of decomposition during tempering are different in these systems. The hexagonal α' decomposes into α phase and incoherent intermetallic compound through several stages in the case of eutectoid systems, while it decomposes directly into equilibrium α and β phases in isomorphous systems, while the β phase heterogeneously nucleates at the lath boundaries and internal substructures [23]. As the composition of α' approaches that of α in equilibrium with β at temperatures low in the $\alpha + \beta$ phase field with time, the β precipitates as fine, isolated, globular particles due to tempering of the martensite (stage 4). Further, cold forming operations only deform the tempered martensitic structure, with neither dynamic recrystallisation nor diffusion of constituent elements. The cold deformation process therefore mainly breaks down the acicular product and increases the dislocation density, resulting in extensive heterogeneous sites for nucleation of α grains. During annealing treatment, recrystallisation of the deformed α results in the formation of equiaxed α grains, while the deformed β particles merely get annealed (stage 5). The primary α grain size is dictated by the 'hold time' during stress relieving treatment and the occasional presence of acicular α suggests incomplete recrystallisation. The above stages yielded a well annealed structure of uniform distribution of nodular β precipitates in a matrix of equiaxed α grains in the $\alpha + \beta$ Ti–5%Ta–1.8%Nb alloy. The above studies have been the basis for adopting this treatment for the industrial scale production of the alloy for component fabrication. This elucidates the role of two stage thermo-mechanical processing in obtaining the equiaxed structure, which could not be restored when the β quenched alloy was isothermally aged in $\alpha + \beta$ phase fields.

Cooling the alloy from temperatures exceeding the T_β resulted either in martensite on quenching or a lamellar $\alpha(+\beta)$ structure termed as 'transformed β' in all cases irrespective of starting with lamellar or equiaxed α. Apart from the above two primary transformations it is recognized that the β phase undergoes a variety of secondary transformations, depending upon the stability of the β phase, which will be described in the next section.

2.2.2 *Phase Transformations of High Temperature β Phase*

The equiaxed $\alpha + \beta$ alloy when quenched from β and $\alpha + \beta$ phase fields resulted in a variety of microstructures

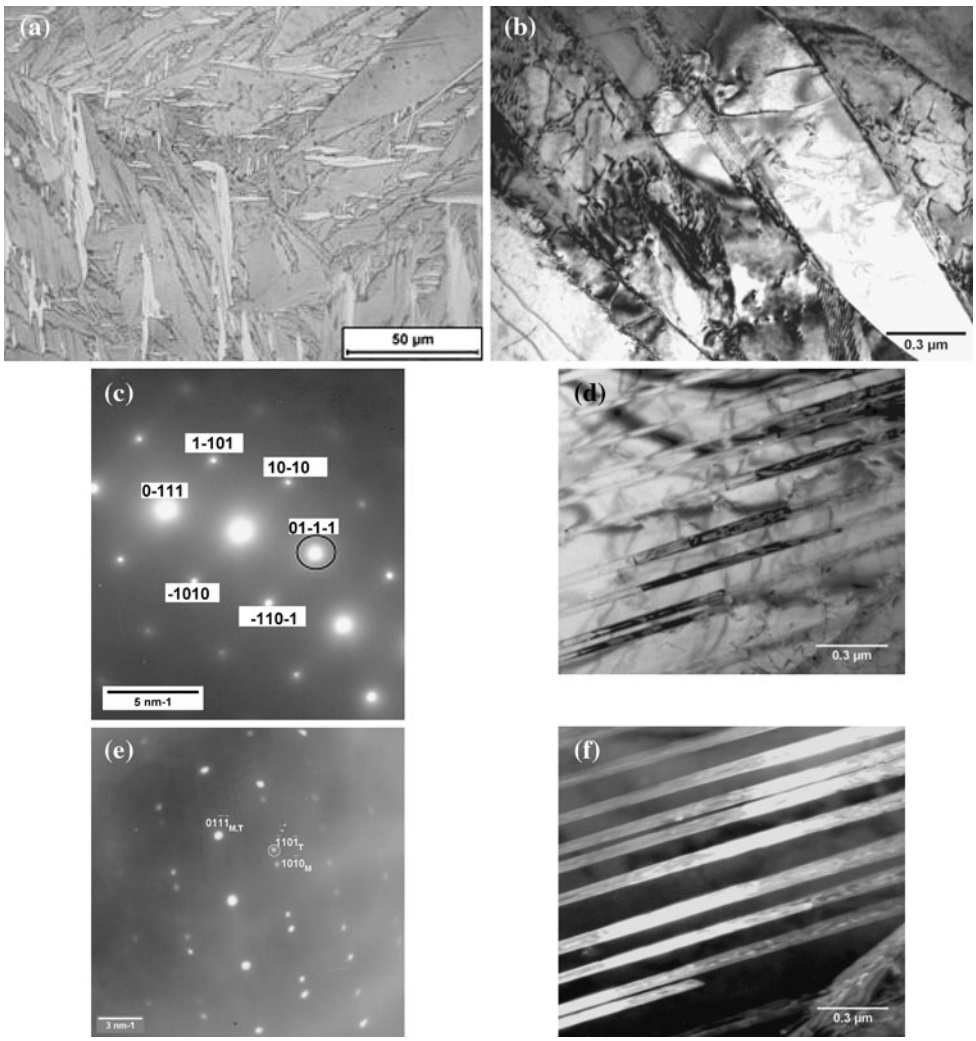

Fig. 7 **a** Optical micrograph showing the martensitic structure after β quenching from 1143 K; **b** TEM bright field micrograph showing lath martensite; **c** SAD pattern along $[1\bar{2}1\bar{3}]_{\alpha'}$ zone axis; **d** coarse internal twins in a plate martensite; **e** SAD pattern along $[1\bar{2}1\bar{3}]_{\alpha'}$ zone axis from this region showing twin reflections; and **f** dark field micrograph showing the $\{0\bar{1}11\}$ type twins with $(0\bar{1}11)$ twin reflection in (**e**) (*circled*)

as a result of different transformation mechanisms, which are described below.

2.2.2.1 Transformation Behavior on Cooling from β Phase Field It is generally observed that the diffusion kinetics in β phase of Ti and its alloys is very high. In fact, abnormal grain growth and related difficulties in weldments as a consequence of high diffusion kinetics have also been reported. Similar trend is displayed even with addition of Ta and Nb in the present Ti–Ta–Nb alloy, with coarse prior β grains of size 2–3 mm, demonstrating the consequence of high diffusion rates in β phase. It is also well established that retention of high temperature β phase is impossible in lean β alloys. The phase transformation of high temperature β phase to a hcp martensite (α') on fast cooling is shown in Fig. 7. Figure 7b, c shows the lath martensite with a dislocation substructure while plate martensite with a twin substructure is seen in Fig. 7d–f. The observation of hexagonal martensite (α') with both lath and plate morphologies observed in the present study confirms the mixed mode of martensitic transformation of parent β phase.

The formation of martensite, their morphology and substructure is known to be influenced by the concentration of β phase [30]. The lath martensite containing a dislocation substructure has been observed in dilute alloys [31]. The laths in a colony belong to a single variant obeying Burgers orientation relationship (BOR). The lath boundaries are found to be low angle boundaries with a misorientation of $<1°$. Twinned plate martensite has also been observed in both Ti and Zr alloys at higher concentrations of β phase. The observation of two types of martensites with lath and plate morphology in the Ti–5Ta–1.8Nb alloy is understandable since the transition is reported to be gradual and can coexist in a certain composition range [32].

The exposure of the alloy to temperatures above β transus followed by slow cooling always resulted in a diffusional product associated with the Widmanstatten transformation as shown in Fig. 5. The slow cooling has favoured the formation of grain boundary α (GBα). GBα

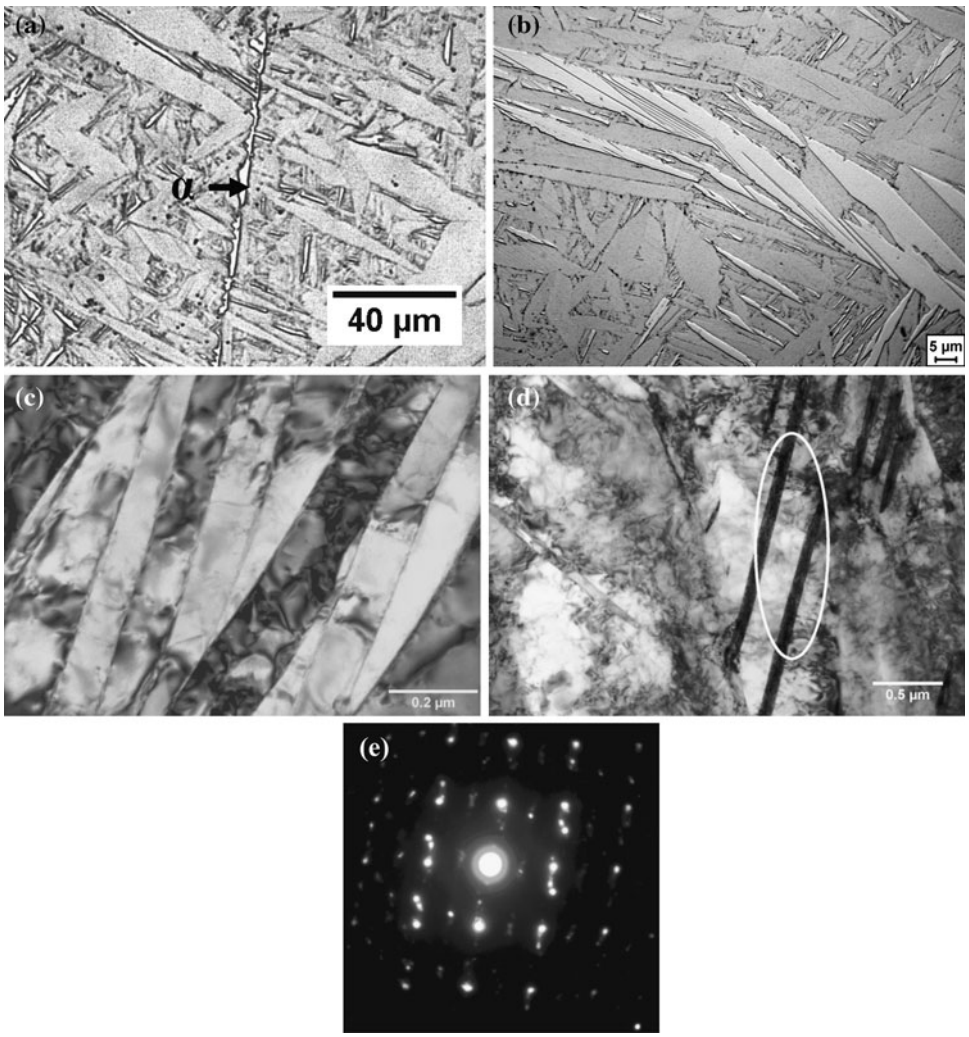

Fig. 8 **a**, **b** Optical micrograph showing a predominantly martensitic structure with fine α grains at the prior β grain boundaries on quenching from 1,133 K; TEM micrograph showing **c** coarse laths of martensite; **d** plate martensite with a twinned substructure (*circled*); and **e** SAD pattern along $[1\bar{1}01]_{\alpha'}$ zone axis containing twin reflections

plates are grain boundary allotriomorphs which are the first to form along the parent β grain boundaries. These α plates possess low interfacial energies between two adjacent β grains. It is observed that the GBα preserves BOR with one of the β grains on either side of it [33], which is also reported in a study by Banerjee et al. [34] in a compositionally graded Ti–8Al–XV sample prepared by a laser deposition technique. It is also reported that the interfacial energy for the nucleation of GBα is lowered by obeying BOR [35]. At very low cooling rates an aligned α colony growth is favoured where a single variant obeying BOR is selected. However, at higher cooling rates finer α plates of multiple variants are selected resulting in a basket weave morphology [36]. The variant selection mechanism operative in this alloy during the Widmanstatten transformation has been studied by texture analysis [37].

2.2.2.2 Transformation of Primary β Phase: Effect of Solute Enrichment Exposure of the alloy at any temperature T in the two phase α + β field produces the equilibrium primary α and β phases designated as α_T and β_T by a diffusional mechanism. The solute concentration, size and amount of primary α_T and β_T are dictated by time and temperature of equilibration. The secondary transformations of primary β_T take place when the alloy is subsequently cooled from temperature T to room temperature. The final room temperature microstructure is however a result of the combination of the primary and secondary transformations. These can best be understood by altering the characteristics of α_T and β_T by changing the equilibration temperature.

Equilibration at high temperatures in α + β phase field would lead to less enrichment of β_T, thereby favouring the martensitic transformation (α') of β_T. The hcp α' is predominantly lath type, with occasional twins. The α_T is retained without any secondary transformation. The transformation products after equilibration at 1133 K in Fig. 8 show lenticular martensite plates within the prior β grains and the primary α phase (α_T) as grain boundary allotriomorphs of α along the prior β boundaries.

It is possible to enhance the solubility limit of Ta and Nb in β_T by lowering the equilibration temperature in α + β

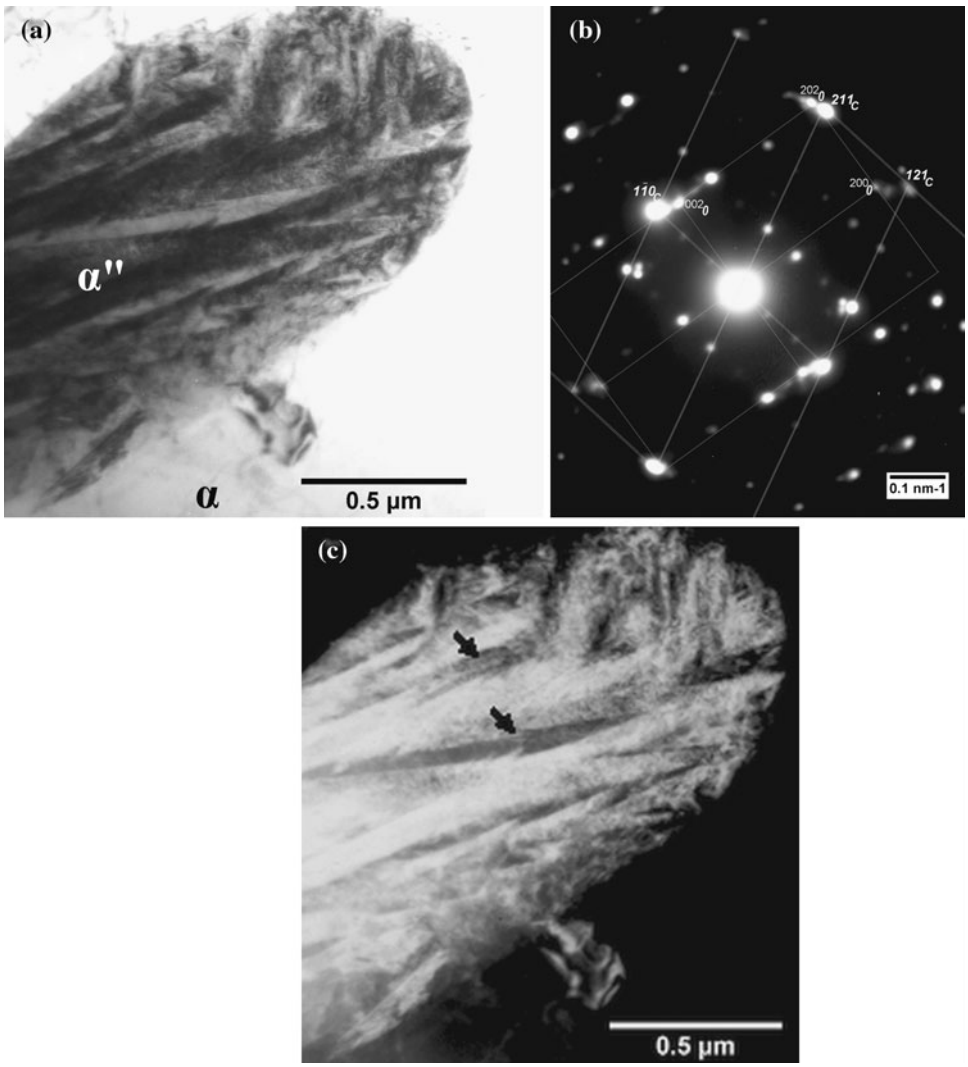

Fig. 9 TEM micrographs of the alloy quenched from 1023 K showing **a** fine plates of α'' martensite in an α grain; **b** SAD pattern of α'' and β phases along $[010]_{\alpha''}$ and $[11\bar{3}]$ zone axis respectively; and **c** dark field micrograph showing fine lenticular plates of α'' (*arrow marked*)

phase field, promoting different types of secondary transformation of β_T. The hcp α' of β_T with less solute content transformed to face centred orthorhombic (f.c.o.) martensite (α'') with increase in solute content at a low equilibration temperature of 1023 K. Figure 9 demonstrates this transformation of β_T.

The transformation behaviour of the alloy on isothermal aging and quenching from $\alpha + \beta$ phase field is summarised as follows:

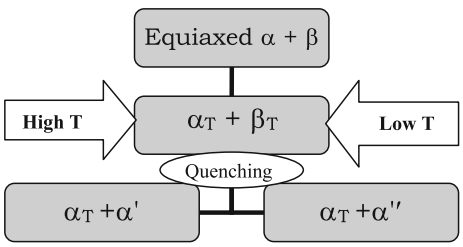

The transition from h.c.p. (α') to orthorhombic (α'') martensite is clearly attributed to the increase in the solute concentration of primary β phase with decrease in equilibration temperature. Reports suggest that α'' is commonly observed in titanium alloys like Ti–Ta, Ti–Nb, Ti–V and Ti–Mo [32] with internal twins along {111} or {110} [38] rather than zirconium alloys. The compositional limit for α' to α'' transition has been reported to be $\sim$4 wt% Mo [39], 10.5 wt% Nb [40] and >22 wt% Ta [41] in Ti–Ta systems.

An interesting observation is the ω phase transformation of certain particles of β phase revealed by a mottled contrast within the β particles as shown in Fig. 10a. The analysis of the SAD pattern in Fig. 10b confirmed the presence of ω phase. The transformation of $\beta \rightarrow \omega$ is well studied [23, 35, 42]. It is known that there are 4 different {111} planes in a cubic system namely (111), $(11\bar{1})$, $(1\bar{1}1)$ and $(\bar{1}11)$ each containing three $\langle 110 \rangle$ directions, which match with the three $<1\bar{2}10\rangle$ directions of ω phase

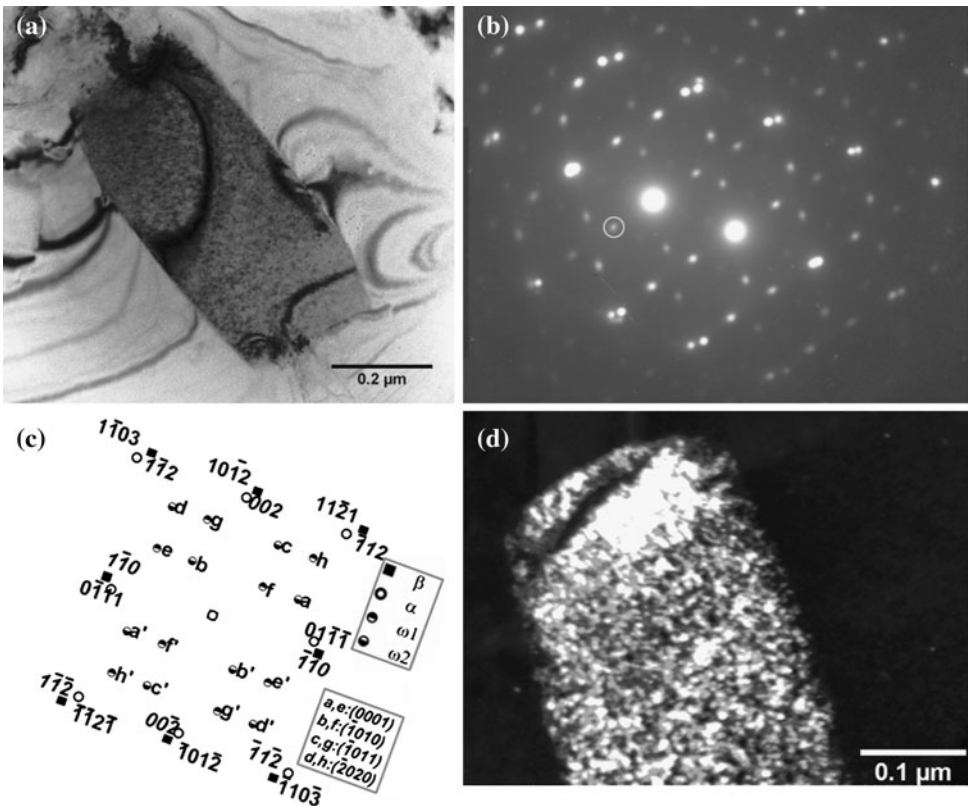

Fig. 10 TEM micrographs of the alloy quenched from 1,023 K showing **a** a mottled contrast of a β particle; **b** SAD pattern along $[110]_\beta$ zone axis with characteristic reflections from two variants of ω phase along $[1\bar{2}10]$ zone axis; **c** key to SAD in (**c**) and **d** dark field micrograph using $(10\bar{1}0)_\omega$ reflection (*circled* in (**b**)) showing fine ellipsoidal ω particles within the β particle in (**a**)

simultaneously. Hence, there are three variants forming on each {111} plane but are equivalent. Therefore, four variants of ω phase form on $\{111\}_\beta$ planes. The SAD pattern in Fig. 10b contains reflections of two variants of ω phase named as ω_1 and ω_2.

The distribution and morphology of ω phase was studied by dark-field microscopy of the ω reflections. Figure 10d shows a dense distribution of fine, ellipsoidal particles with size ranging from 4 to 10 nm. This suggests that athermal ω has formed, since isothermal ω which forms by a diffusional process [42] is reported to be solute lean compared to β phase. Athermal ω is also reported to form with an ellipsoidal morphology, with their long axis along $\langle 111 \rangle_\beta$, while isothermal ω can be ellipsoidal or cuboidal, depending upon the misfit between β and ω phases. It is known that isothermal ω forms in Zr and Ti alloys when aged at temperatures below 773 K, which is also the upper limit of temperature for ω phase precipitation by ageing. Based on these considerations, the ω phase observed in this alloy during quenching from temperatures higher than 773 K can be termed as athermal ω. The co-existence of α'' and ω phase has also been observed in several regions.

The coexistence of martensite and ω has been reported in the metastable Ti–10V–2Fe–3Al alloy with a Ms temperature of about 828 K [43]. The coexistence of α'' and ω is attributed to the compositional dependence of the Ms and ω start temperatures, which decrease with progressive increase in composition of β phase [44] and the overlap of a narrow range of composition of formation of α'' and ω phases [30]. If the equilibration of the alloy is carried out at very low temperatures in the $\alpha + \beta$ phase field, the β_T is highly enriched with β stabilizing elements Ta and Nb to such an extent that β_T does not undergo any secondary transformation. Based on these studies, the transformation sequence at different temperatures can be summarized as follows:

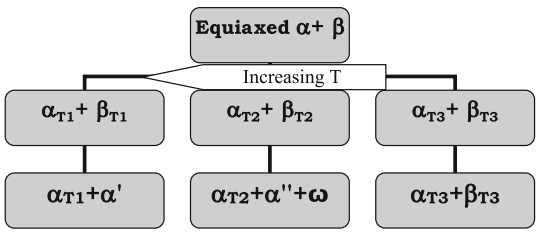

The systematics of secondary transformation of primary β phase is summarized as follows:

- The transformation mode of β changes from martensitic to Widmanstatten with decrease in cooling rate.
- The decomposition mode of primary β phase is influenced by its solute content at different temperatures in the $\alpha + \beta$ phase field.
- The primary β phase undergoes secondary transformation to α', α'', ω or retained β depending upon solute enrichment, which can be artificially introduced by altering the equilibration temperature in the $\alpha + \beta$ phase field.

The studies on transformation behavior of the Ti–5%Ta–1.8%Nb alloy provided an in-depth understanding of the various transformation mechanisms that the alloy undergoes. This study provided a means to obtain desired features in the microstructure that would provide the best combination of corrosion and mechanical properties. The alloy also exhibited interesting texture behavior, typical of hcp alloys. The next section gives a detailed description of the texture that evolved in the ternary alloy during processing stages such as rolling and wire drawing, severe plastic deformation and also during transformation of the high temperature β phase.

2.3 Texture in the Ti–Ta–Nb Alloy

HCP metals like Ti, Zr and their alloys exhibit strong tendencies to develop textures, during forming operations, recrystallisation and phase transformation. Anisotropy of the crystal lattice, stacking fault energy, c/a ratio and processing parameters like temperature, mode and extent of deformation and strain rate dictate the nature of deformation texture [45]. It is essential to understand the synergy between these factors, to tailor the properties of new systems. Gey and Humbert [46] had reported that when commercially pure Ti (CP-purity $\sim$99.85%) is β annealed after unidirectional deformation (such as cold rolling), the β phase inherits a strong $\{112\}\langle 111\rangle$ type of texture, while without the initial cold rolling, no specific β phase texture was observed. The Ti–5Ta–1.8Nb alloy exhibited deformation and transformation texture, which has been studied in detail by X-ray diffraction and EBSD technique.

2.3.1 *Deformation and Transformation Textures in Ti–Ta–Nb Alloy*

It is known that Ti and its alloys exhibit three different types of textures: deformation, recrystallisation and transformation textures. These three types of texture are not independent of each other. For example, recrystallisation texture of β is known to depend on the pre-existing deformation texture. Similar process is true for texture during transformation of high temperature β to α on cooling. These factors are well demonstrated in the Ti–Ta–Nb alloy in this section. It is demonstrated that the deformation texture of Ti–Ta–Nb alloy depends crucially on the type of deformation (i-e) rolling or wire drawing. The conventional X-ray diffraction methods are used for preliminary suggestive experiments, backed up by detailed EBSD observations for detailed study of micro-mechanisms.

The normalized intensity of the XRD peaks is the chosen signature of texture, while the XRD peak intensity of powder pattern was used as reference. Significant difference was observed in the relative peak intensity of

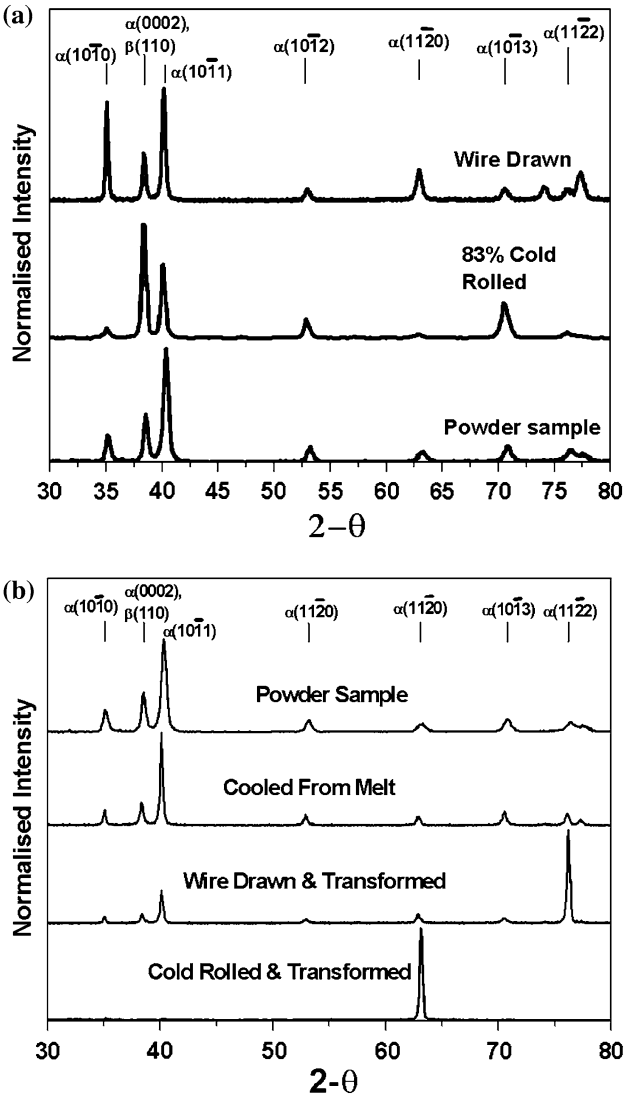

Fig. 11 XRD patterns in Ti–5Ta–1.8Nb using Cu–Kα incident radiation showing **a** deformation texture, with different modes of deformation, unidirectional cold rolling (83% reduction) and wire drawing and **b** products of $\beta \rightarrow \alpha + \beta$ transformation with different histories, namely cold rolling, wire drawing and melting, compared with the powder pattern

deformed samples in comparison to the powder sample as shown in Fig. 11a. The strongest (100%) peak for the cold rolled sample is seen at 38.4°, which corresponds to $(0002)_\alpha$ as well as $(110)_\beta$, whereas the 100% peak for the powder sample is at 40.1° corresponding to $(10\bar{1}1)_\alpha$. Therefore, the observed shift of the peak with 100% intensity from $(10\bar{1}1)_\alpha$ in the powder sample to $(0002)_\alpha$ in the cold rolled sample indicates a preferential orientation due to deformation and is referred to as 'deformation texture'. The wire drawn sample shows maximum enhancement of peak intensity for a different crystallographic plane, namely $(10\bar{1}0)_\alpha$. This indicates a different type of deformation texture in the wire drawn alloy, from that of

the cold rolled sample [47]. Similar basal plane $(0002)_\alpha$ type of deformation textures have been reported for cold rolled Ti and other hcp metals [48, 49], which indicate that the deformation textures differ in case of cold rolled and wire drawn alloy due to difference in the nature of applied stress.

The transformation texture introduced during β to $\alpha + \beta$ transformation on slow cooling of the high temperature β phase is found to be influenced by the deformation texture existing prior to annealing in β phase field. The evidence for such possible "memory" of deformation texture during recrystallisation of β phase and subsequent transformation was clear from the behaviour of β to $\alpha + \beta$ transformation in (a) cold rolled (b) wire drawn and (c) weld with no deformation history [47].

The XRD patterns from a $\alpha + \beta$ structure obtained after slow cooling of the β phase starting with three different histories like: (a) cold rolled, (b) wire drawn (DD section) and (c) weld-possessing no deformation history are shown in Fig. 11b along with that from powder sample for comparison. It is seen that the cold rolled and transformed (CRT) alloy shows a single strong peak for $(11\bar{2}0)_\alpha$ while the wire drawn and transformed (WDT) alloy shows the strongest peak for the $(11\bar{2}2)$ plane, which is attributed to a preferential orientation, referred to as 'transformation texture'. It is observed that there is not only a complete modification of the deformation textures during $\beta \rightarrow \alpha + \beta$ transformation, but the transformation texture is also dependent on the mode of deformation. This aspect is further confirmed by the observation of complete absence of texture in weld region, which undergoes the transformation of liquid $\rightarrow \beta \rightarrow \alpha + \beta$. The random orientations observed in a sample cooled from liquid state suggest that an initial deformation is essential to obtain a textured transformation product.

2.3.2 *Study of Microtexture by Electron Back Scattered Diffraction*

EBSD offers a powerful means of studying the mechanism of selection of orientations at the microscopic level during the Widmanstatten transformation of β to $\alpha + \beta$. Very often, the majority of α lamellaein a Widmanstatten product of $\alpha + \beta$ possesses similar orientations (Fig. 12a, b). Similar feature holds good for β lamellae also. Even if the $\alpha + \beta$ lamellae form across two β grains, the orientation of the α lamellae remained unchanged. The presence of α lamellae with similar crystallographic orientation on either side of prior β grain boundary provided direct evidence for the texture in this alloy. The presence of grain boundary allotriomorph α in Fig. 12a delineates the two β crystals, $\beta 1$ and $\beta 2$.

The average behaviour of many α and β lamellae could be mapped onto pole density contours. The suggestion

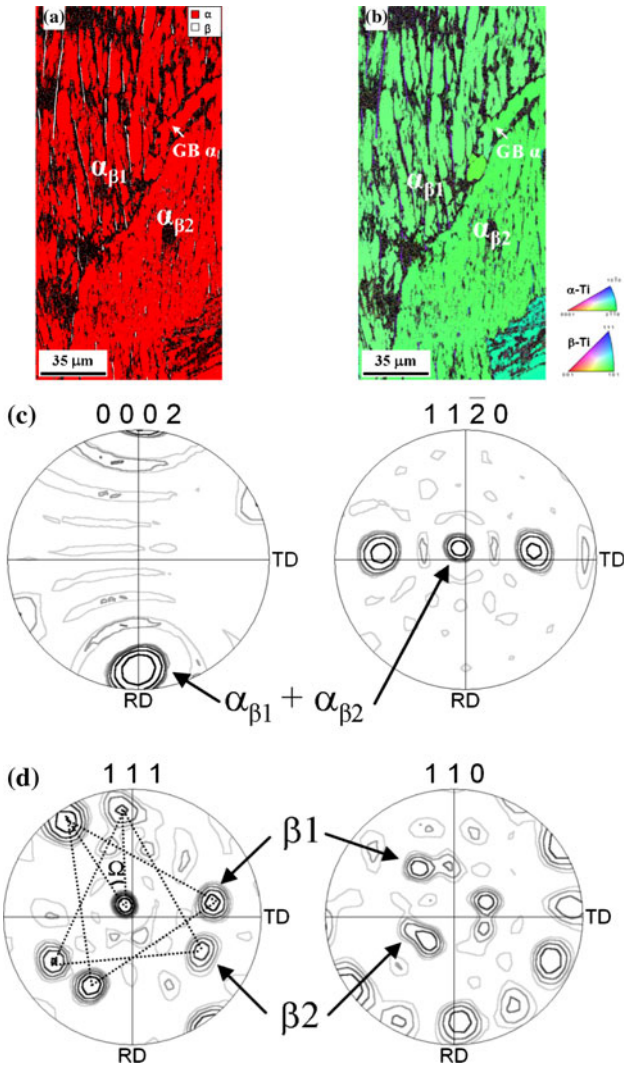

Fig. 12 EBSD images and pole figure contours of Ti–Ta–Nb alloy solution treated in the β phase field and slow cooled. Gβ α refers to grain boundary α, which demarcates the boundary between two parent β grains and $\alpha_{\beta 1}$ and $\alpha_{\beta 2}$ refer to the α phase that formed from the prior β grains $\beta 1$ and $\beta 2$, respectively; **a** phase identification map; **b** crystal orientation map of α and β-Ti (coded as *green* and *blue*); **c** pole concentrations along (0002) and $(11\bar{2}0)$ plane normal for α-Ti phase; and **d** pole concentrations along the (111) and (110) plane normals for the β-Ti phase. (Color figure online)

from preliminary XRD observations could be further confirmed by observation of high concentration of (0002) poles along rolling direction (RD) and $(11\bar{2}0)$ along the sample normal direction (ND) (Fig. 12c). Similar exercise for the β phase suggests the 'crowding' of the pole density contours along (111) and (110) plane normals (Fig. 12d) in accordance with expected BOR. It is possible to infer based on symmetry considerations that of the two parent β crystals, one aligned along RD and another with an angle of misorientation Ω with it. It is also shown that the misorientation angle between the two parent β crystals dictate the deviation from obeying the BOR. It is seen here that the

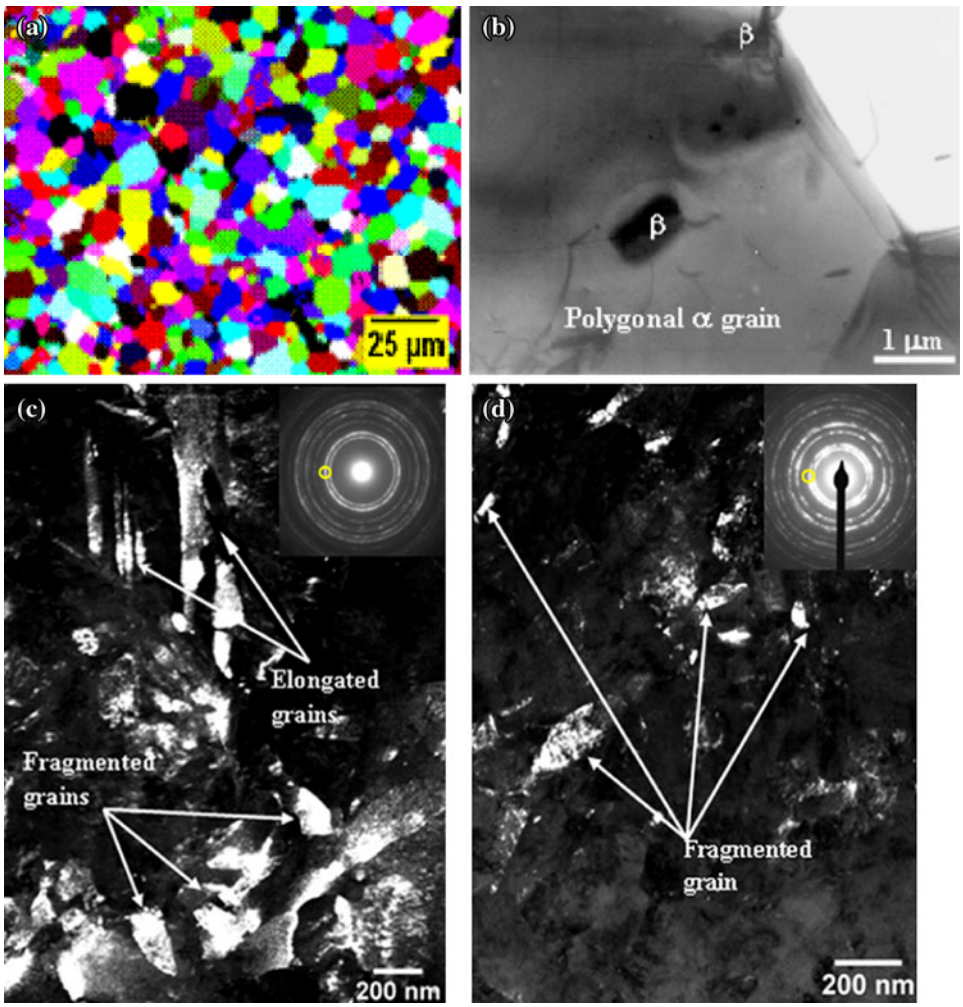

Fig. 13 **a** EBSD image of the alloy before cryo-rolling showing equiaxed grains of about 8 μm; **b** TEM bright field image showing the presence of fine β particles in the matrix; and **c**, **d** TEM dark field image after 85% unidirectional room temperature and cryo-rolling showing fragmented α-Ti grains. (Color figure online)

orientation of $\alpha_{\beta 1}$, where BOR is obeyed, has prevailed over that of $\alpha_{\beta 2}$, where BOR is only partially obeyed. This is probably due to the diffusion controlled transformation mechanism operating in this system. The GBα nucleating at the prior β/β boundary follows BOR for any one of the two β grains (say $\beta 1$). Further α lamellae growing out of GBα that has already nucleated with preferential orientation maintains the same orientation although this amounts to deviations from BOR (for $\beta 2$). This is made possible by the diffusion distances, which are much larger during diffusional transformation than required for strict adherence to BOR. Detailed analyses of these studies are published elsewhere [33].

2.3.3 *Microstructure and Microtexture Evolution During Severe Plastic Deformation*

Grain refinement through severe plastic deformation is a novel attempt made to achieve high ductility and yield strength (YS) [50, 51] in the Ti–Ta–Nb alloy. Heavy deformation by severe cold working such as cryo rolling has been employed for fragmenting the grains followed by annealing to stabilize the microstructure. The mechanism of grain fragmentation during SPD and the resultant microstructure and texture showed interesting features, which are described in brief in this section.

SPD up to 85% at room temperature had changed the original random distribution of equiaxed α grains of 8 μm size into elongated grains together with few fragmented grains, while deformation at sub-zero temperatures led to complete fragmented grain of 50–250 nm size as shown in Fig. 13. Consequently, the hardness and hence the strength are expected to be doubled. Despite such significant changes, there is no sign of texture within α grains during SPD.

The sub-grains tend to orient randomly and thus lose the acquired texture due to deformation. Such a behavior was observed beyond about 50% of cold working where, the intensity ratio once again approaches that of the powder pattern, possibly due to fragmentation of the grains as early as 50% of cold working at sub-zero temperatures. Figure 14 shows the EBSD micrograph of the 85% cold rolled sample after annealing at 773 K for 2 h demonstrating the

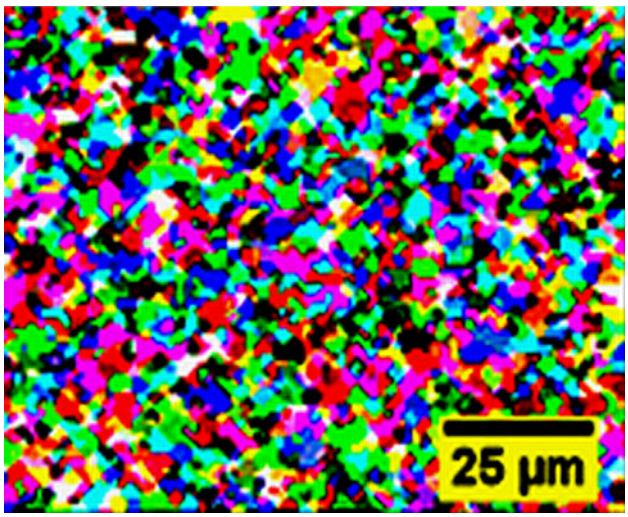

Fig. 14 EBSD micrograph after annealing at 773 K for 2 h showing equiaxed sub-micrometer grains. (Color figure online)

stability of refined equiaxed grain structure at 773 K. The presence of equiaxed sub-micrometer grains is clearly seen, which demonstrates that grain refinement has been achieved and the microstructure is stable at 773 K [52]. This method offers a novel way to achieve high strength by grain refinement (<1 μm) through SPD by cryo-rolling. However, the effect of SPD on corrosion behavior needs to be studied.

The mechanism of texture evolution during deformation and transformation in the Ti–Ta–Nb alloy is well understood. The influence of texture on the corrosion behavior is not obvious, since the alloy inherently possesses excellent corrosion resistance (<1 mpy). The alloy has been developed for operations in aqueous medium of concentrated nitric acid where the temperatures are not expected to exceed 120°C. Hence, the high temperature strength was of no concern. The mechanical properties were evaluated for the first time for the alloy [53] and it was found that YS was about 330 MPa and ultimate tensile strength (UTS) exceeded 400 MPa with a ductility of 30% in the 'as processed' condition. The design requirement based on ASTM standard for mechanical properties of pure titanium which is generally employed for corrosion applications [54] is YS in the range 275–400 MPa, UTS ~345 MPa and ductility ~20%. This shows that the alloy meets the design requirements. The corrosion behavior of the alloy in correlation with the microstructure is described in the next section.

2.4 Corrosion Behavior of Ti–5Ta–1.8Nb Alloy

Corrosion resistance of titanium alloys is mainly influenced by the chemistry of the alloy. Additional improvement in corrosion resistance is possible by altering the microstructure, especially morphology and distribution of phases, which in turn is controlled by the alloying elements or temperature and the cooling rate [22, 23]. The available industrial experience of commercially pure Ti with Fe (impurity) content ≥0.05% shows that failure in nitric acid occurs mainly in welds due to preferential attack along the interface of α-β lamellae in weld. This has been attributed to the segregation of Fe and formation of Fe-rich intermetallics [55]. Hence, reduction in Fe content to <0.05% was a major incentive in the indigenous development of the alloy, which has offered a manifold improvement in corrosion resistance as compared to CP-Ti.

The corrosion resistance of Ti–5%Ta–1.8%Nb alloy could further be improved by altering the morphology of Widmanstatten product $\alpha + \beta$, from lamellar structure to uniform distribution of β particles in an equiaxed α matrix (see Sect. 2). The average corrosion rate of the lamellar and equiaxed structures (Figs. 6, 7) in the liquid phase of 11.5 M boiling nitric acid was estimated as 1.5 and 0.3 (±0.1 mpy) (Fig. 15) respectively [56, 57]. The latter morphology could reduce the corrosion rate by five times. These values are far less than the corrosion rate of the present generation materials like 304L SS which is nearly 180 mpy or CP-Ti which is nearly 5 mpy [58], which establishes that the Ti–Ta–Nb alloy has excellent corrosion resistance. The superior corrosion resistance of equiaxed microstructure with a homogeneous distribution of β particles over a lamellar or acicular product is also reported in the Ti weld [55].

The possible reason for the above observation is as follows: The acicular microstructure consisting of alternate lamellae of α and β phases with solute repartitioning between the two, leads to the formation of periodic micro-galvanic cells, which is deleterious [55]. The periodic microchemical variation is avoided when the β phase is distributed as fine particles in the equiaxed α matrix, which explains for the superior corrosion resistance of this structure.

Not withstanding the influence of microstructure discussed above, the improvement of corrosion resistance of Ti and its alloys is mainly due to the chemical effect of alloying elements. The high corrosion resistance due to addition of Nb and Ta has been rationalized as follows: the pentavalent nature of Nb and Ta, comparable atomic radius, as Ti, the low solubility in oxidizing media and stabilization of the oxide film.

Further, a systematic study on the influence of microstructure on corrosion resistance of the alloy in the three phases of nitric acid namely liquid, vapor and condensate, has been carried out in our laboratory, to arrive at the best microstructure with best corrosion resistance or in other words to optimize the process flow chart for the alloy. A mechanistic understanding of the formation of stable oxide film on the surface which is protective has also been attained, which will be described in the subsequent sections.

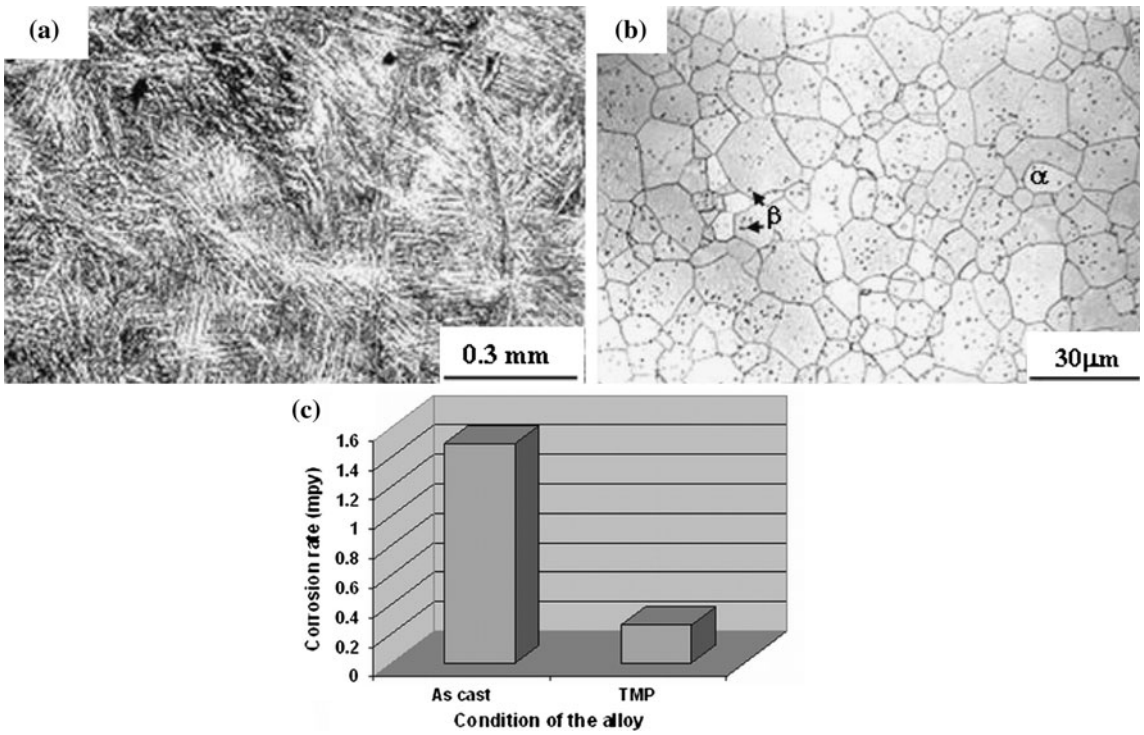

Fig. 15 Optical micrographs of alloy showing **a** lamellar transformed β structure in as cast condition; **b** equiaxed α grains with fine β particles after thermo-mechanical processing; and **c** comparison of corrosion rates in the liquid phase of boiling 11.5 M nitric acid

2.4.1 *Corrosion Control Through Design of Microstructure*

Further enhancement in corrosion resistance could be achieved through additional manipulation of the microstructures with respect to the amount, morphology and distribution of the constituent phases by appropriate heat treatments [59, 60], which in turn modified the oxide film characteristics. Several conventional, industrial heat treatments [61] like mill annealing, solution treatment and solution treatment followed by aging/overaging were adopted. The corrosion behavior of the resultant microstructures are compared in Fig. 16, based on which an optimum treatment has been identified for processing of this alloy.

The corrosion rates measured in the liquid, vapor and condensate phases of boiling 11.5 M nitric acid for the different microstructures (Fig. 16) suggests the following trends.

Although the differences in absolute values are quite low in many measurements the trend in corrosion rates from the figure is very clear.

- The liquid phase showed lowest corrosion rate and condensate phase the highest with vapor phase being intermediate for all microstructures.
- The order of increase in corrosion rate in liquid phase was *aging* $\approx$ *overaging* $\approx$ *Solution Treatment (ST)* $<$ *Mill Annealing (MA)* $\approx$ *Initial condition*, which changed to *overaging* $\approx$ *aging* $<$ *MA* $\approx$ *Initial condition* $<$ *ST* in the vapor and condensate phases.
- The alloy in solution treated and aged or overaged condition yields the maximum corrosion resistance in all phases of nitric acid.

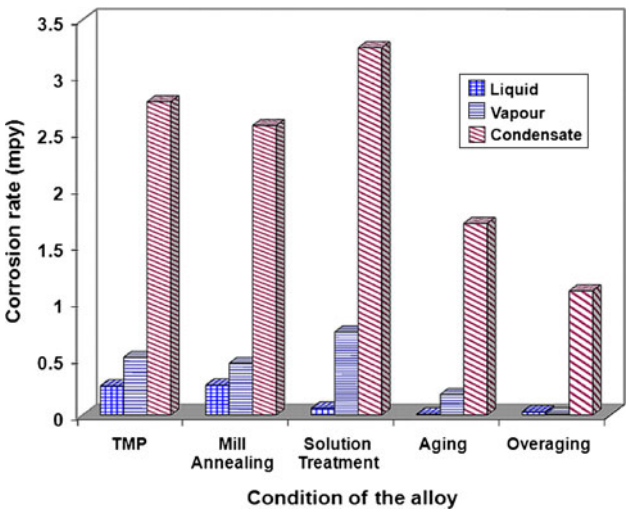

Fig. 16 Comparison of three phase corrosion rates of the alloy with different microstructures. (Color figure online)

The above results show that although the Ti–5%Ta–1.8%Nb alloy exhibits the best corrosion resistance

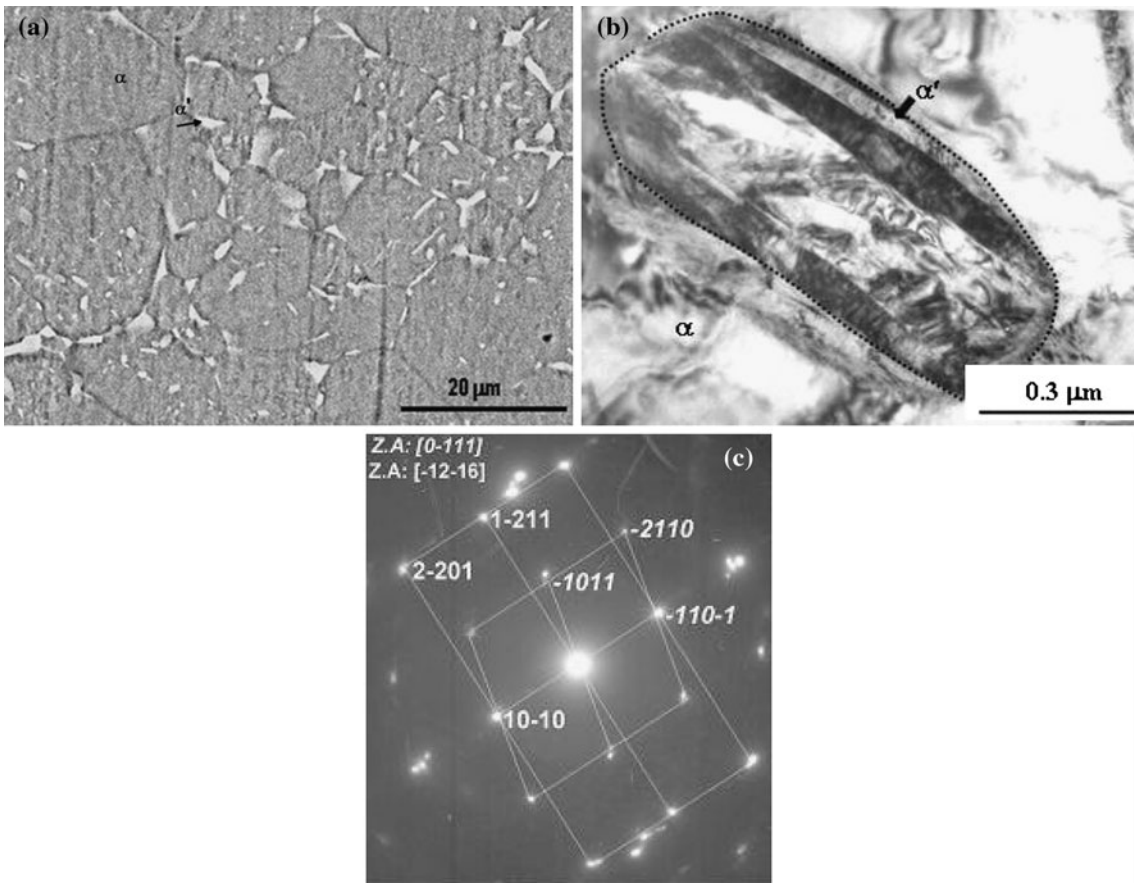

Fig. 17 Microstructure after solution treatment for 2 h at 1113 K **a** BSE image showing predominantly equiaxed structure and intra and intergranular α' (β); **b** TEM micrograph showing well resolved α' laths in an intragranular β particle (*marked*); and **c** SAD pattern from primary α along $[0\bar{1}11]$ and h.c.p. α' along $[\bar{1}2\bar{1}6]$ zone axis

(<1 mpy) when it is subjected to a heat treatment consisting of solution treatment at 1,113 K, high in the $\alpha + \beta$ phase field followed by aging or overaging treatments in the temperature range of 823–973 K [58]. The microstructures that resulted from the different treatments have been examined to identify the microstructural feature that influences the corrosion behavior. These studies were useful in arriving at following inferences:

(1) Presence of martensite (α') in solution treated alloy (Fig. 17) increases the corrosion rate, which could be understood due to the acicular morphology of martensite and a stress assisted dissolution of the metal.
(2) Considerable reduction in corrosion rate could be achieved by either aging (823/873 K) or overaging (973/1023 K) of the solution treated alloy (Fig. 18).

It is clear that presence of fine β precipitates aid in improving the corrosion resistance of the alloy, while presence of strained acicular phases is deleterious, since their interfaces could act as potential anodic sites. The assessment of corrosion behavior in the liquid, vapor and condensate phases of nitric acid has led to the identification of the key microstructural parameters that exert an influence, as nature, volume fraction, size, distribution and composition of different co-existing phases. Apart from microstructure, another important aspect was the role of environment in the corrosion behavior which is discussed below.

2.4.2 *Role of Oxidizing Medium on the Corrosion Behavior*

The consistently higher corrosion rate of the Ti–Ta–Nb alloy in the vapor and condensate phases in contrast to liquid phase of boiling 11.5 M nitric acid (51% concentration) irrespective of the microstructure has been understood as follows: It has been reported that the corrosion rate of Ti in nitric acid is strongly influenced by the oxidizing potential of the acid which increases with concentration. The maximum corrosion rate occurs around a concentration of 40–50% (9–11.25 M) [62] as seen in Fig. 19a. Purity of the nitric acid also plays a role with the presence

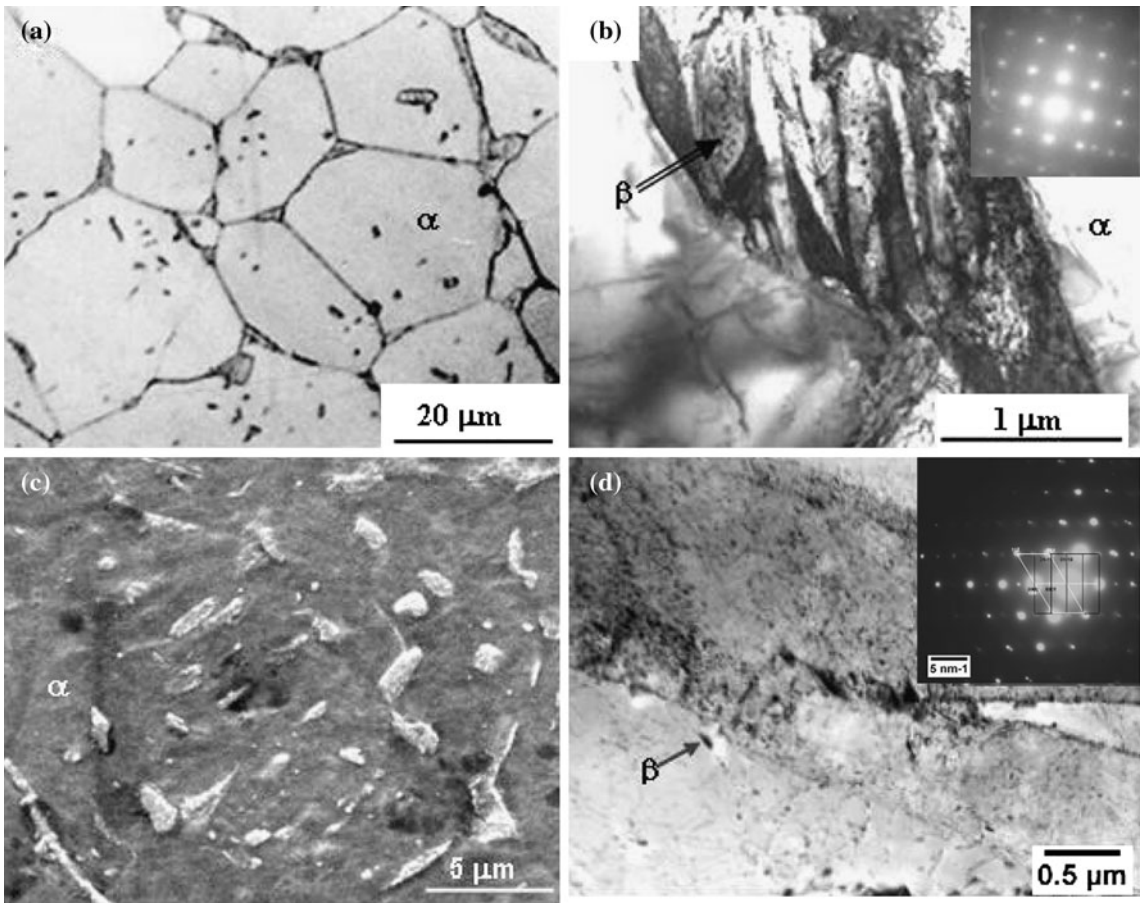

Fig. 18 **a** Optical micrograph showing a predominantly α matrix on aging at 823 K; **b** TEM micrograph showing fine precipitates of β due to tempering of martensite (*inset* shows SAD from $[100]_{\beta}$); **c** SEM micrograph showing uniform distribution of fine β precipitates in a predominantly α matrix in the alloy overaged at 973 K; and **d** TEM micrograph showing evidence for formation of slightly coarser β precipitates during tempering of martensite at 973 K (*inset* shows SAD from $[11\bar{1}]_{\beta}$ and $[2\bar{1}\bar{1}0]_{\alpha}$ zone axis

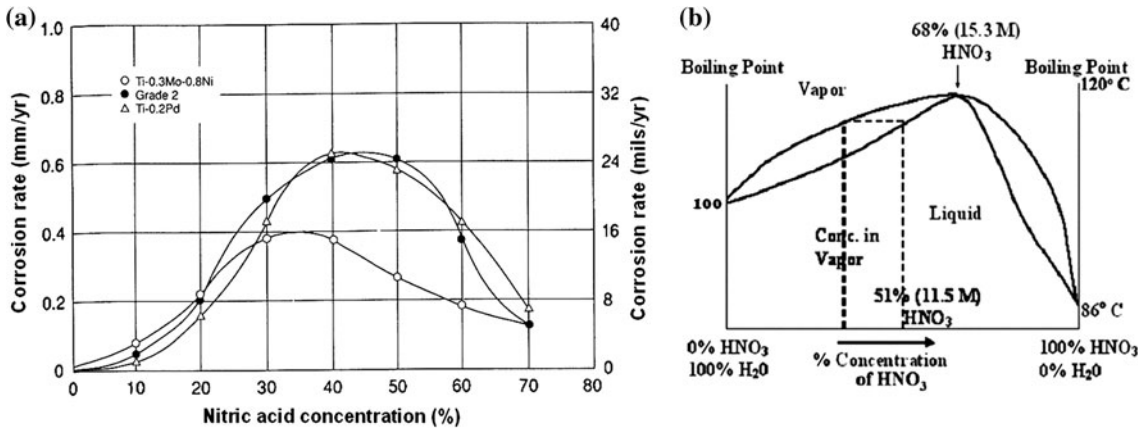

Fig. 19 **a** Corrosion of Ti and Ti alloys in boiling nitric acid, for a total period of 480 h, the solution renewed every 24 h [62] and **b** nitric acid–water phase diagram [64] with tie line at the boiling point of 11.5 M nitric acid showing a lower concentration in vapor phase than liquid prior to azeotropic temperature

of relatively small amounts of certain dissolved metallic ions like Fe^{3+}, Cr^{6+}, Ti^{4+} [62] and Si^{4+} [63], effectively inhibiting the high temperature corrosion of Ti in nitric acid. Further, the dissolved Ti ions themselves act as self inhibitors that reduce the corrosion rate of Ti by formation of TiO_2 by the following reactions.

$$Ti \rightarrow Ti^{3+} + e^{-}$$

$$Ti^{3+} \rightarrow Ti^{4+} + e^{-}$$

$$Ti^{4+} + 2H_2O \rightarrow TiO_2 + 4H^{+}$$

It is understandable that in the absence of dissolved titanium ions like in flowing conditions such as in vapor and condensate phases, the alloy exhibits high corrosion rates. In such conditions, the oxide essentially consists of Ti_2O_3 as reported to form by the following reactions.

$$Ti \rightarrow Ti^{3+} + e^{-}$$

$$2Ti^{3+} + 3H_2O \rightarrow Ti_2O_3 + 6H^{+}$$

High corrosion rates in flowing conditions also show that Ti_2O_3 is less protective than TiO_2 [64].

The concentration of nitric acid in vapor phase in equilibrium with liquid phase is lower (27% or 6 M) as seen in the phase diagram of nitric acid and water [64] (Fig. 19b). Comparing with Ti, it is expected that the high oxidizing potential at higher concentrations should also have increased the corrosion rate in the liquid phase than in the vapor phase. However, it is realized that some alloying elements cause a shift in the peak of corrosion rate versus concentration of nitric acid towards lower concentrations as shown in Fig. 19a for two alloys namely Ti–0.2Pd and Ti–0.8Mo–0.3Ni and the extent of shift depends upon the nature and concentration of the alloying element. Although such information is not available for Ti–5%Ta–1.8%Nb alloy, considering that Ta and Nb are β stabilizers, it is reasonable to expect that the behaviour would be similar to addition of Pd and Mo as shown in Fig. 19a. Hence, it is quite reasonable to understand that the higher corrosion rates measured in the vapor and condensate phases is due to the lower concentration of nitric acid, in contrast to liquid phase.

Further, the renewal of the solution after 48 h during the corrosion testing provides the self inhibiting effect due to dissolved titanium ions in the liquid phase, leading to the formation of TiO_2, which is beneficial to decrease the corrosion rate. The lowest corrosion rate in the liquid phase can therefore be attributed to the combined effect of the high oxidising potential [58] of the 11.5 M (51%) nitric acid and the self-inhibition effect due to dissolved Ti^{4+} ions, which promotes the formation of passive TiO_2 film. Along the same lines, the slightly higher corrosion rate in the vapor phase is attributed to the weakly oxidizing nature of the acid despite the inhibiting effect due to dissolved titanium ions. The highest corrosion rate in the condensate phase arises not only due to the low concentrations or low oxidizing potential similar to vapor phase but also absence of accumulated inhibiting titanium ions due to continued removal of the metal surface layers [64] resembling the flowing liquid phase. Under flowing conditions, the oxide film that forms is also not stable.

Although both microstructure and oxidizing nature of the medium play important roles, there is no common agreement in literature w.r.t the effect of β phase on corrosion resistance of titanium alloys. It is reported that, though single phase titanium alloys are most resistant to corrosion in general, $\alpha + \beta$ alloys provide a good combination of corrosion resistance and mechanical properties [63]. Yu and Scully [65] observe that β solution treated Ti–15Mo–3Nb–3Al exhibits a better corrosion resistance as compared to the aged microstructure, due to repartitioning of the alloying elements during aging process. But Thair [66] reports that a microstructure with both α and β phases in Ti–6Al–7Nb alloy exhibits better corrosion resistance than β treated alloy, which has been rationalized in terms of the differences in the characteristics of the oxide film. These studies suggest that corrosion behavior is influenced by a combination of the following factors:

- Temperature, concentration and purity of the acid.
- Self inhibition effect of dissolved ions.
- Nature of alloying additions.
- Microstructure of the alloy.
- Nature and stoichiometry of the oxide.

The last factor namely, the nature and stoichiometry of the oxide is described in the next section.

2.4.3 *Characteristics of the Oxide Film in Ti–5%Ta–1.8%Nb Alloy*

Extensive literature on the effect of solutes in the titanium oxide lattice has shown that generally titanium forms *n*-type oxide namely TiO_2 [67]. Due to presence of anion vacancies some of the Ti^{4+} ions are replaced by Ti^{3+} ions to maintain electrical neutrality, making the TiO_2 film non-stoichiometric [67]. The above theory, well established for high temperature oxidation is also reported to be valid for aqueous corrosion in Ti alloys [64]. The role of constituent phases is also important in the context of their influence on the nature of the oxide film following the underlying microstructure, difference in the kinetics of formation and passivity of the different oxides and the role of alloying elements in the dissolution rate of titanium. These mechanisms in relation to the nature of oxide film are discussed in this section. The characteristics of the oxide film like surface morphology, thickness, microstructure and composition have also been studied in the alloy, which is also described in detail below.

2.4.3.1 Thickness of Oxide Film The thickness of the oxide film, an index of the propensity of the Ti–Ta–Nb alloy to corrode in different environments has been

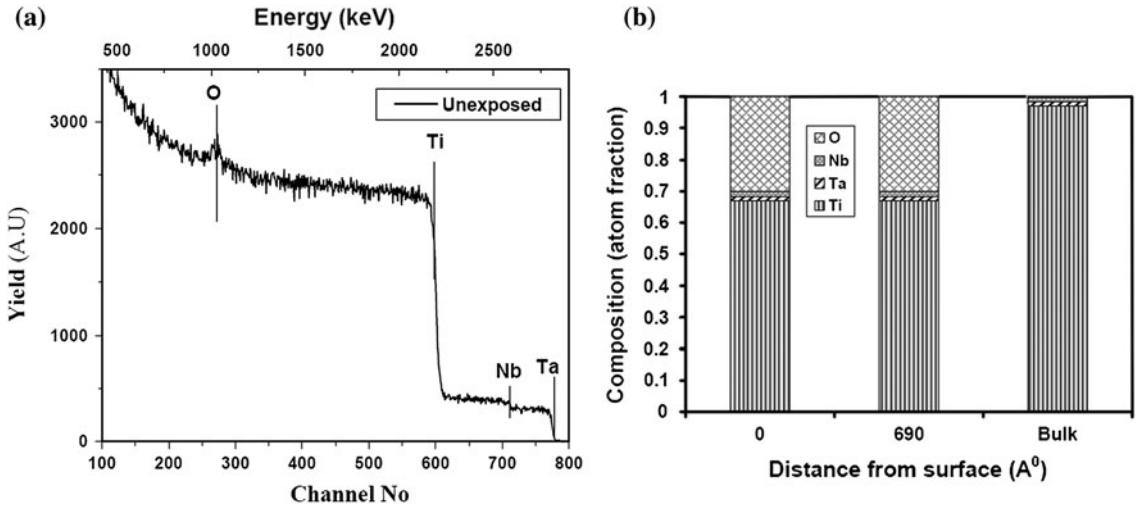

Fig. 20 **a** RBS spectrum from the surface of the alloy unexposed to nitric acid showing Ti, Ta and Nb edges and O peak corresponding to the native oxide layer and **b** histogram showing the variation of composition of the oxide film as a function of distance from the surface calculated from the spectrum in (**a**)

evaluated from the Rutherford Backscattering Spectroscopy (RBS) experiments through a composition depth profiling. A typical RBS spectrum from the unexposed alloy is shown in Fig. 20a. The peak corresponding to oxygen and edges corresponding to Ti, Ta and Nb are observed suggesting their presence both on the surface and in the alloy. Based on the assumption that the oxide formed is TiO_2, the thickness of the oxide layer was estimated as $\sim$690 Å as shown in Fig. 20b. The thickness of the oxide layer in the corrosion tested specimen in vapor and condensate phase was estimated to be 1740 and 2340 Å respectively [68]. It is observed that, despite higher thickness of the oxide layer after condensate phase corrosion as compared to vapor phase, it is not protective as is evident from the higher corrosion rate. This has been understood based on weakly oxidising nature of the condensate phase resulting in a porous oxide layer [58].

2.4.3.2 Microstructure of the Oxide Film The morphology, structure and type of the oxide film has a direct bearing on the corrosion resistance of a material for a given environment. A typical TEM micrograph of the oxide film is shown in Fig. 21a. Interestingly, the oxide film is a mixture of amorphous and nanocrystalline phases (Fig. 21b, c) of size 10–100 nm. Although, distinction between anatase and rutile could not be made by diffraction analysis of crystalline regions, the low temperature of formation (aqueous medium $\sim$120°C), suggests that it could be anatase (Fig. 21b), which is stable at temperatures below 973 K. It has also been reported that anatase forms on exposure to boiling nitric acid of 50% concentration [69]. But the presence of small amounts of other oxides of titanium, tantalum and niobium cannot be excluded due to closely spaced 'd' values of some of these phases. However, careful analysis of the electron diffraction patterns suggested the possible presence of difference oxides of Ti and Nb along with Ta_2O_5. The observation of orthorhombic nanocrystalline Ta_2O_5 has also been reported by Harvey and Wilman [70], when Ta was anodized in HNO_3 and heat treated at 973 K. These results suggest that the oxide formed consists of nano-crystalline anatase and Ta_2O_5 in an amorphous matrix [68].

2.4.3.3 Composition of the Passive Oxide Film The oxide layer was analyzed using surface analytical techniques such as RBS and X-ray photoelectron spectroscopy (XPS). The RBS spectra showed that the concentration of Ta and Nb on the surface of alloy subjected to condensate and vapor phase corrosion is higher than in the unexposed alloy, suggesting lower dissolution of Ta and Nb as compared to Ti in vapor and condensate phases of nitric acid, which is in tune with the high corrosion rates measured in these phases [56, 68].

Typical XPS spectra of the alloy exposed to vapor and condensate phases and unexposed alloy are shown in Fig. 22. Two closely lying peaks at binding energies of 458 and 464 eV are clearly seen in the spectra from the unexposed alloy. It is known that the $2p^{3/2}$ and $2p^{1/2}$ doublet peaks of metallic titanium occur at 453.9 and 460 eV respectively, which are expected to shift to higher binding energies, maintaining the doublet separation energy, with increase in the oxidation state of titanium. Hence, the peaks observed at 458 and 464 eV can be correlated to $2p^{3/2}$ and $2p^{1/2}$ levels of TiO_2. The presence of TiO_2 in the unexposed alloy is attributed to the native oxide layer [68] formed on the alloy surface.

In the alloy exposed to vapor phase, apart from TiO_2, presence of Ta_2O_5 and Nb_2O_5 was confirmed from the

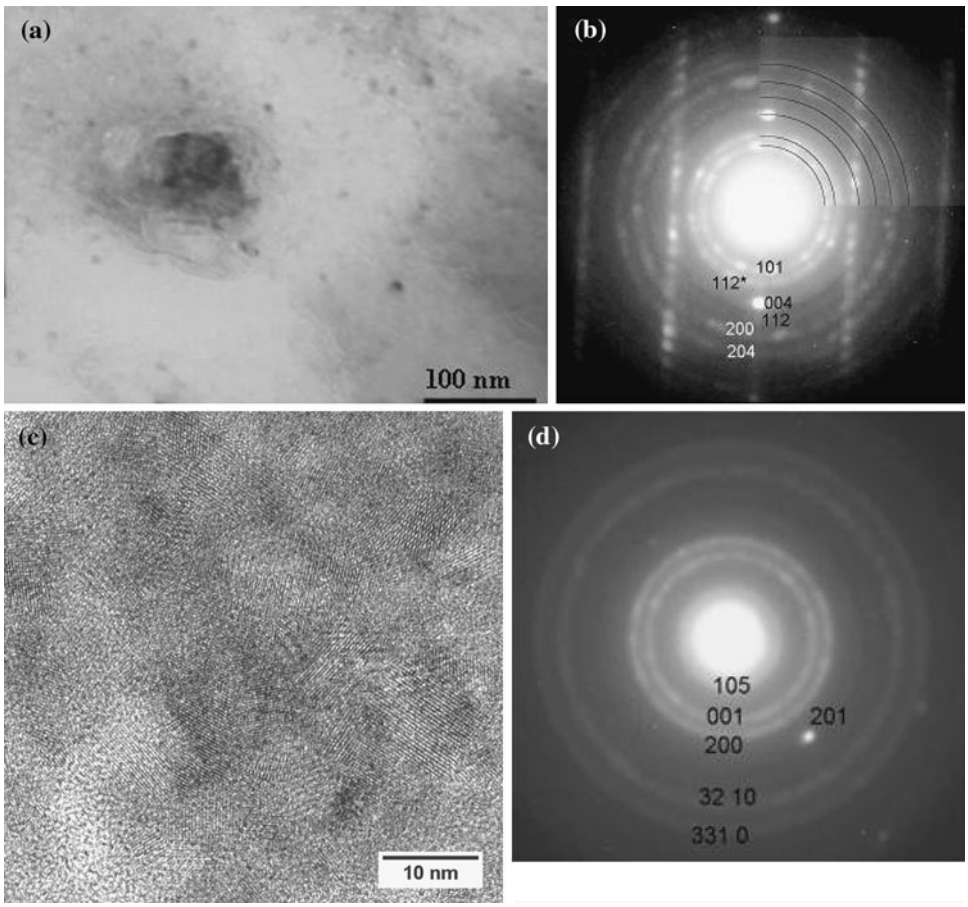

Fig. 21 **a** TEM micrograph showing nano-crystalline nature of the oxide film; **b** SAD pattern corresponding to anatase (*asterisk* corresponds to 112 Ti_2O_3/NbO_2); **c** HREM image of the oxide film showing a mixture of amorphous and crystalline regions; and **d** SAD showing the presence of Ta_2O_5

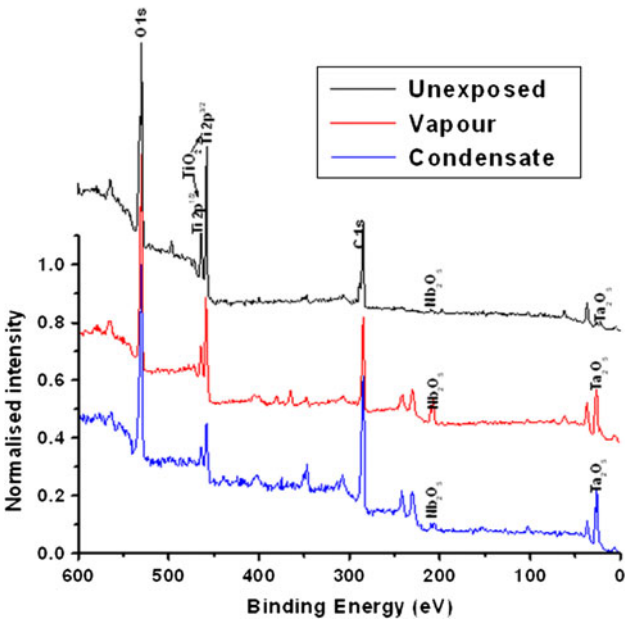

Fig. 22 XPS survey spectra from the solution treated and overaged alloy in the unexposed condition and after three phase corrosion test showing the presence of TiO_2 in all cases and increased amounts of Ta_2O_5 and Nb_2O_5 in the alloy exposed to vapor and condensate phases. (Color figure online)

peaks observed at appropriate binding energies (Fig. 23). Presence of Nb_2O_5 was observed in lower amounts in both vapour and condensate phases compared to Ta_2O_5 [68]. In addition, parallel electron energy loss spectroscopy (PEELS) analysis of the oxide film of the alloy exposed to vapour phase corrosion suggested formation of lower oxides of Ti.

A similar observation is made in the case of condensate phase also, but with a higher intensity of Nb_2O_5 and Ta_2O_5 peaks. A similar behavior of increased amounts of Ta and Nb was observed in the RBS spectra also. These results support the formation of Ta_2O_5 and Nb_2O_5 in the vapor and condensate phases of nitric acid [44].

The formation of stable TiO_2 strengthens the fact that the absence of inhibitor effect due to flowing acid is responsible for the higher corrosion rate in the condensate phase. The increasing amounts of Ta_2O_5 and Nb_2O_5, also suggest that these are stable oxides, while TiO_2 that forms on the surfaces is washed away due to flowing conditions of the acid, exposing a fresh metal surface. This is quite understandable since Ta_2O_5 and Nb_2O_5 are more stable than TiO_2 as Ta and Nb themselves possess higher corrosion resistance than Ti. The characteristics of the oxide film can be summarized as follows:

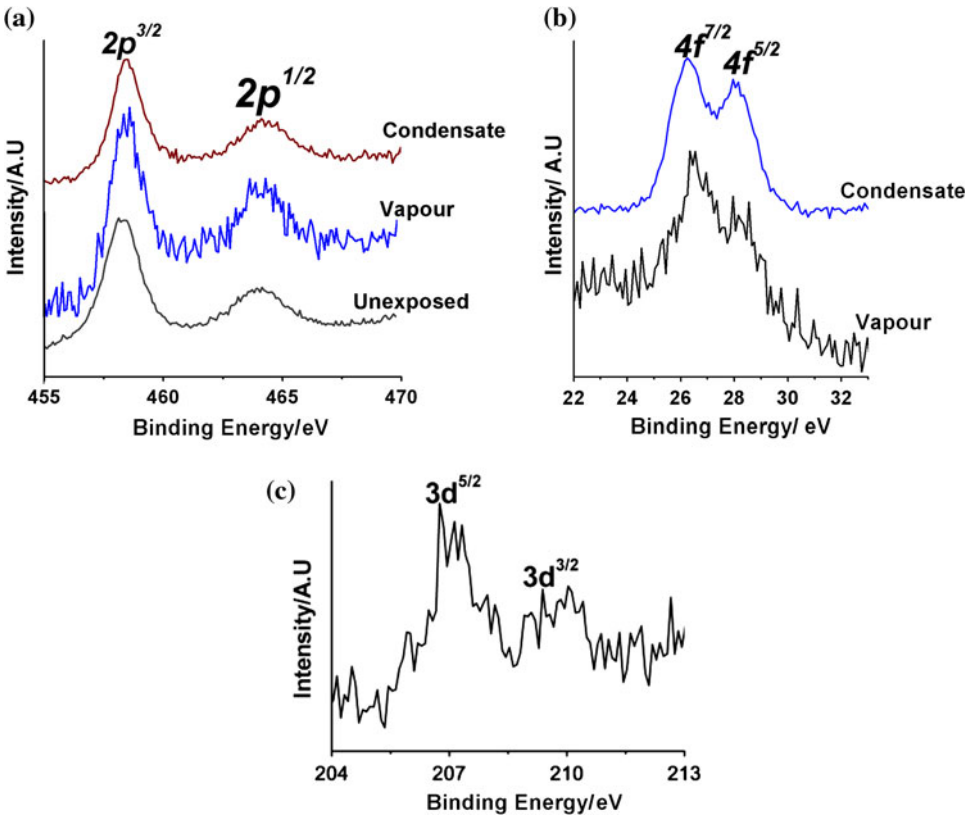

Fig. 23 High resolution XPS spectra from the alloy (after sputtering) XPS spectra showing the presence of **a** TiO_2 in before and after exposure to vapour and condensate phases; **b** Ta_2O_5 after exposure to vapour and condensate phases; and **c** Nb_2O_5 after exposure to condensate phase. (Color figure online)

- Predominantly TiO_2 namely anatase formed on the alloy surface prior to and after exposure to nitric acid along with low amounts of lower oxides of Ti.
- The presence of low amounts of less passive lower oxides is understood in the light of weakly oxidising conditions in vapor and condensate phases, that increases the corrosion rate.
- The increased amounts of Ta_2O_5 and Nb_2O_5 on the surface on exposure to condensate phase suggests the higher dissolution of Ti due to the absence of inhibitor effect under flowing conditions in a weakly oxidising acid.

The three phase corrosion behavior of the Ti–5%Ta–1.8%Nb alloy in boiling nitric acid has been studied and the factors contributing to its high corrosion resistance have been identified. The corrosion resistance of the alloy with different microstructures is a manifestation of the combined effect of nature of alloying elements, microstructure of the alloy, concentration and dynamic conditions of the acid and the nature of the oxide film under the prevailing conditions.

The weldability of the alloy has also been established [71] to be as good or even better than for Ti/Ti joints. The weld also possesses the required mechanical strength and has exhibited corrosion rates <5 mpy [72]. Dissimilar welds between Ti–Ta–Nb alloy and SS304L by explosive cladding have also shown that the welds are sound, meet the design requirements with respect to mechanical properties and exhibit corrosion rates less than 10 mpy [73]. Further, the interface is free of intermetallics. The interface is also corrosion resistant when tested in boiling 11.5 M nitric acid.

The above studies demonstrate that the Ti–5Ta–1.8Nb has enormous potential as a structural material for use in highly oxidizing media such as the nuclear spent fuel reprocessing plant, where electro-oxidative reactions would be involved in the separation. The elaborate studies on this alloy have successfully culminated in the usage of this alloy in the form of filler wires for the fabrication of the dissolver component.

Titanium alloys have emerged to be competitive materials for use in various process industries in recent years, the major limitation being its high processing cost. The principal cost drivers have been identified as raw material processing, melt processing, and fabrication. Hence, several approaches have been identified [74–78] to minimise the cost of titanium products such as:

- continuous method to win titanium,
- direct consolidation of won titanium into useful products without traditional melting,
- single melt processes,
- greater use of scrap,

- near-net-shape fabrication processes,
- alternate compositions using cheaper elements, and
- relaxed compositional requirements.

All strategies require the accompanying relevant property data base to support implementation, although there is no significant change in the basic alloy design principles. The first step has been to produce the titanium alloys continuously, in which the reduction reaction and the melting of the product spongy titanium are simultaneously carried out. Drawing the titanium/its alloys to semi-finished products from the melt has also been successfully demonstrated. Most of the recent investigations are anchored around systems that are developed in the five decades of the twentieth century. The trends in many recent investigations pertain to replacement of costly elements like tantalum, niobium and vanadium by cheaper elements and attempt to evaluate the acceptability of the alloy with higher oxygen content than before.

3 Summary

The present overview highlights the design principles of materials in the development of Ti–5Ta–1.8Nb alloys for corrosion resistance applications. The development of Ti–Ta–Nb alloy carried out in authors' laboratory for reprocessing applications has been explained in detail. The indepth understanding on phase transformation mechanisms and the governing factors have been successfully employed to tailor the microstructure through appropriate selection of process conditions to enhance the corrosion resistance. The different types of texture that the alloy exhibits, the detailed study on the nature of oxide films that form during different types of corrosion and a comprehensive understanding of the corrosion mechanism in the developmental alloy are explained. The economics of titanium production is identified as the major cause for the titanium alloys being not as popular as aluminium or steels. It is concluded that the successful use of Ti alloys with unique combination of properties lies in the ability of metallurgists to identify cost effective processes for production and fabrication.

References

1. Anantharaman T R, *Rustless Wonder: Research on Iron Pillar at Delhi*, Vigyan Prasar Publications, New Delhi (1999).
2. Schutz R W, in *Corrosion Tests and Standards: Application and Interpretation, ASTM Manual Series: MNL 20*, (ed) Baboian R, ASTM, Philadelphia (1995), p 493.
3. Froes F H, Yau T-L, and Weidinger H G, in *Materials Science and Technology: A Comprehensive Treatment*, (eds) Cahn R W, Haasen P, and Karamer E J, *Vol. 8, Structure and Properties of Non ferrous Alloys*, K. H. Matucha, VCH, Weinheim (1996), p 399.
4. Collings E W, in *Alloying* (eds) Walter J L, Jackson M R, and Sims C T, ASM International, Metals Park, OH (1988), p 257.
5. Lampman S, in *Metals Handbook, Vol. 2, Properties and Selection: Nonferrous Alloys and Special-Purpose Materials*, 10th edn., ASM International, Metals Park, OH (1990), p 592.
6. Gogia A K, *Def Sci J* **55** (2005) 149.
7. McCann M, and Fanning J, in *Handbook of Mechanical Alloy Design*, (eds) Totten G, Xie L, and Funatani K, Marcel Dekker Inc., New York (2004), p 539.
8. Ramanujan R V, *Int Mater Rev* **45** (2000) 217.
9. Kamachi Mudali U, Dayal R K, and Gnanamoorthy J B, *J Nucl Mater* **203** (1993) 73.
10. Kiuchi K, Hayakawa H, Takagi Y, and Kikuchi M, in *Proceedings of the Fourth International Conference on Nuclear Fuel Reprocessing and Waste Management, RECOD'94*, Vol. III, London, April 24–28, (1994).
11. Otero E, Pardo A, Saenb E, Utrilla M V, and Hierro P, *Corros Sci* **38** (1996) 1485.
12. Balbaud F, Sanchez G, Fauvet P, Santarini G, and Picard G, *Corros Sci* **42** (2000) 1685.
13. Motooka T, and Kiuchi K, *Corrosion* **58** (2002) 703.
14. Raj B, and Kamachi Mudali U, *Prog Nucl Energy* **48** (2006) 283.
15. Nagano H, and Kajimura H, *Corros Sci* **38** (1996) 781.
16. Yau T L, in *Industrial applications of Titanium and Zirconium, ASTM STP 917*, (eds) Young C S, and Durham J C, ASTM, Philadelphia (1986), p 57.
17. Kamachi Mudali U, Dayal R K, and Gnanamoorthy J B, *J Mater Eng Perform* **4** (1995) 756.
18. Kato C, Motooka T, and Kiuchi K, in *Proceedings of the Fifth International Conference on Nuclear Fuel Reprocessing and Waste Management (RECOD-98)*, Vol. 3, France (1998), p 852.
19. Nagano H, Kajimura H, and Yamanaka K, *Mater Sci Eng A* **198** (1995) 127.
20. Leduc M, Duigou A L, and Pelras M, in *Industrial Applications of Titanium and Zirconium, ASTM STP 917*, (eds) Young C S, and Durham J C, ASTM, Philadelphia (1986), p 69.
21. Motooka T, and Kiuchi K, *Mater Trans* **43** (2002) 1220.
22. Murakami Y, in *Titanium '80: Science and Technology, Proc. Fourth International Conference on Titanium*, (eds) Kimura H, and Izumi O, The Metallurgical Society of AIME, Warrendale (1980), p 153.
23. Willians J C, in *Titanium Science and Technology*, (eds) Jaffee R I, and Burte H M, Vol. 3, Plenum Press, New York (1973), p 1433.
24. Mythili R, Thomas Paul V, Saroja S, Vijayalakshmi M, and Raghunathan V S, *Mater Sci Eng A* 390 (2005) 299.
25. Gill F J, Genebra M P, Manero J M, and Planell J A, *J Alloys Compd* **329** (2001) 142.
26. Bania P J, in *Beta Titanium Alloys in the 1990's*, (eds) Eylon D, Boyer R, and Koss D A, TMS, Warrendale, Pennsylvania (1993), p 3.
27. Duwez P, *Trans ASM* **45** (1953) 934.
28. Dobromyslov A V, and Elkin V A, *Scr Mater* **44** (2001) 905.
29. Semiatin S L, Seetharaman V, and Weiss I, *J Met* (1997) 34.
30. Collings E W, in *Materials Properties Handbook—Titanium Alloys*, (eds) Boyer R, Welsch G, Collings E W, and Scott W, ASM International, Materials Park, OH (1998), p 1.
31. Banerjee D, and Muraleedharan K, *Philos Mag A* **77** (1998) 299.
32. Dobromyslov A V, *Mater Sci Forum* **546–549** (2007) 1349.
33. Karthikeyan T, Arup Dasgupta, Saroja S, Vijayalakshmi M, Khan A J, Bhattacharjee D, and Raghunathan V S, *Mater Sci Eng A* **485** (2008) 581.
34. Banerjee R, Collins P C, Bhattacharya D, Banerjee S, and Fraser H L, *Acta Mater* **51** (2003) 3277.

35. Banerjee S, and Mukhopadhyay P, *Phase Transformations: Examples from Titanium and Zirconium Alloys*, Elsevier, Amsterdam (2007), p 557.
36. Flower H M, *Mater Sci Technol* **6** (1990) 1082.
37. Karthikeyan T, Dasgupta A, Khatirkar R, Saroja S, Samajdar I, and Vijayalakshmi M, *Mater Sci Eng A* **528** (2010) 549.
38. Mackenzie K, and Bowles J S, *Acta Metall* **5** (1957) 137.
39. Davis R, Flower H M, and West D R F, *J Mater Sci* **14** (1979) 712.
40. Bagariatskii Y A, Nosova G I, and Tagunova T V, *Sov Phys Dokl* **3** (1959) 1014.
41. Bywater K A, and Christian J W, *Philos Mag* **25** (1972) 1249.
42. Hickman B S, *J Mater Sci* **4** (1969) 554.
43. Toran J R, and Biederman R R, in *Titanium' 80: Science and Technology, Proceedings of the Fourth International Conference on Titanium*, (eds) Kimura H, and Izumi O, The Metallurgical Society of AIME, Warrendale (1980), p 1491.
44. Mythili R, *Study of Ti–5Ta–1.8Nb Alloy: Microstructure and Its Influence on Corrosion and Mechanical Properties*, Ph D Thesis, University of Madras, May (2009).
45. Singh A K, and Schwarzer R A, *Mater Sci Eng A* **307** (2001) 151.
46. Gey N, and Humbert M, *Acta Mater* **50** (2002) 277.
47. Karthikeyan T, Dasgupta A, Saroja S, Khatirkar R, Vijayalakshmi M, and Samajdar I, *Mater Sci Eng A* **485** (2008) 581.
48. Philippe M J, Serghat M, van Houtte P, and Esling C, *Acta Met Mater* **43** (1995) 1619.
49. Zhu Z S, Gu J L, and Chen N P, *Scr Metall* **30** (1994) 605.
50. Wang Y, Chen M, Zhou F, and Ma E, *Nature* **419** (2002) 912.
51. Lee Y B, Shin D H, Park K-T, and Nam W J, *Scr Mater* **51** (2004) 355.
52. Dasgupta A, Laha K, Kayalvizhi R, Raju S, Murugesan S, Saroja S, Sarma V S, and Vijayalakshmi M, *Proceedings of the MRS Fall Meeting: Symposium—EE: Nano- and Microscale Materials—Mechanical Properties and Behaviour Under Extreme Environments in Boston*, MA, USA, Dec. 1–5 (2008).
53. Mythili R, Saroja S, Vijayalakshmi M, and Raghunathan V S, *Mater Sci Eng A* **454–455** (2007) 43.
54. ASTM-B367-06, ASTM International, Philadelphia (2006).
55. Witton, *Corrosion Resistance of Titanium*, Imperial Metal Industries, Birmingham (1969).
56. Mythili R, Saroja S, Vijayalakshmi M, and Raghunathan V S, *J Nucl Mater* **345** (2005) 167.
57. Karthikeyan T, Mythili R, Saroja S, and Vijayalakshmi M, *Met Mater Process* **18** (2006) 282.
58. Mythili R, Ravi Shankar A, Saroja S, Raju V R, Vijayalakshmi M, Dayal R K, Raghunathan V S, and Balasubramaniam R, *J Mater Sci* **42** (2007) 5924.
59. Brossia C S, and Cragnolino G A, *Corrosion* **57** (2001) 768.
60. Fukuzuka T, Shimogori K, Satoh H, and Kamikubo F, in *Titanium'80: Science and Technology, Proceedings of the Fourth International Conference on Titanium*, (eds) Kimura H, and Izumi O, The Metallurgical Society of AIME, Warrendale (1980), p 2783.
61. Lampman S, in *ASM Metals Hand book, Vol. 2, Properties and Selection: Nonferrous Alloys and Special-Purpose Materials*, 10th edn., ASM International, Materials Park, OH (1987), p 592.
62. Schutz R W, and Thomas D E, in *Metals Handbook, Vol. 13, Corrosion*, 9th edn., ASM International, Materials Park, OH (1987), p 669.
63. Bomberger H B, in *Industrial Applications of Titanium and Zirconium, STP 830*, (eds) Webster R T, and Young C S, ASTM, Philadelphia (1984), p 143.
64. Furuya T, Kawafuku J, Satoh H, Shimogori K, Aoshima A, and Takeda S, *ISIJ Int* **31** (1991) 189.
65. Yu S Y, and Scully J R, *Corrosion* **53** (1997) 965.
66. Thair L, *Studies on Thermomechanically Processed and Nitrogen Ion Implanted Ti–6Al–7Nb Biomedical Alloy*, Ph D Thesis, Anna University, Chennai, India (2002).
67. Trethway K R, and Chamberlain J, *Corrosion for Students of Science and Engineering*, Wiley, New York (1988), p 335.
68. Mythili R, Saroja S, and Vijayalakshmi M, *Mater Charact* **61** (2010) 1326.
69. Ogawa S, and Watanabe D, *Sci Rep Res Inst Tohoku Univ Ser A Phys Chem Metall* **7** (1955) 184.
70. Harvey J, and Wilman H, *Acta Crystallogr* **14** (1961) 1278.
71. Karthikeyan T, Dasgupta A, Saroja S, Vijayalakshmi M, and Raghunathan V S, *J Nucl Mater* **335** (2004) 299.
72. Dasgupta A, Karthikeyan T, Saroja S, Raju V R, Vijayalakshmi M, Dayal R K, and Raghunathan V S, *J Mater Eng Perform* **16** (2007) 800.
73. Sudha C, Prasanthi T N, Murugesan S, Saroja S, Kuppusami P, and Vijayalakshmi M, *Sci Technol Weld Join* **16** (2011) 133.
74. Suzuki R O, *J Met* (2007) 68.
75. Moxson V S, and Froes F H, *J Met* (2001) 39.
76. Destefani J D, in *Metals Handbook, Vol. 2, Properties and Selection: Nonferrous Alloys and Special-Purpose Materials*, 10th edn., ASM, Metals Park, OH (1992), p 586.
77. Klug K L, Ucok I, Gungor M N, Guclu M, Kramer L S, Tack W T, Nastac L, Martin N R, and Dong H, *J Met* (2004) 35.
78. Lutjering G, and Williams J C, *Titanium*, Springer, Berlin (2003), p 84.